Nonlinear Phase Noise in Dispersion Unmanaged Fiber-Optic Systems

NONLINEAR PHASE NOISE IN DISPERSION UNMANAGED FIBER-OPTIC SYSTEMS

BY

SABER RAHBARFAM, M.Sc.

A THESIS

SUBMITTED TO THE DEPARTMENT OF ELECTRICAL & COMPUTER ENGINEERING

AND THE SCHOOL OF GRADUATE STUDIES

OF MCMASTER UNIVERSITY

IN PARTIAL FULFILMENT OF THE REQUIREMENTS

FOR THE DEGREE OF

MASTER OF APPLIED SCIENCE

Master of Applied Science (2018) McMaster University

(Electrical & Computer Engineering) Hamilton, Ontario, Canada

TITLE:	Nonlinear Phase Noise in Dispersion Unmanaged Fiber-Optic Systems
AUTHOR:	Saber Rahbarfam M.Sc., (Electrical Engineering) McMaster University, Hamilton, Canada
SUPERVISOR:	Dr. Shiva Kumar
NUMBER OF PAGES:	xiv, 93

I wholeheartedly dedicate this thesis to my beloved parents, whose moral and emotional consolation and their encouragement has planted the seed of knowledge in me and they keep nurturing it by their everlasting support.

Abstract

Since the introduction of optical fibers in 1960's in communication systems, researchers have encountered many challenges to improve the signal quality at the receiver as well as transmitting the signal as distant as possible. The former was achieved by employing coherent receivers, which let us use M-array modulation formats, such as QPSK, or QAM, and polarization of the signal. The later is accomplished by the advent of optical amplifiers. Optical amplifiers enable us to compensate for the loss occurred within the fiber optic line, without the need for optical-electrical signal conversion. These amplifiers add noise to the line which interacts with the nonlinearity in the fiber line. This interaction causes phase change in the propagating signal called nonlinear phase noise, which degrades the system performance.

In this study we will derive an analytical expression for the linear and nonlinear phase noise variance in dispersion unmanaged fiber optic systems, using a first-order perturbation theory. We use numerical examples to depict the proposed system performance in terms of nonlinear phase noise variance. We will conclude that the nonlinear phase variance in a dispersion unmanaged system is much lower than the corresponding noise variance in a dispersion managed system. We will use this concept and will introduce more dispersion in the line by adding fiber brag gratings (FBGs) throughout the fiber link. Through numerical simulations, we will illustrate

the improvement we get by adding FBG in each span. We will show that employing FBG improves the system performance for systems working at symbol rates 5 GBaud, which we get the best improvement to less than 20 GBaud, and beyond 20 GBaud there will be no improvement.

Nowadays, telecommunication systems based on fiber optics are working at symbol rates around 28 GBaud. We will introduce new models to reduce the nonlinear phase, by splitting digital back propagation (DBP) between transmitter and receiver, and using optical phase conjugation (OPC) in the line. We will prove that the new proposed models lower the phase noise variance significantly, for single pulses. We will also illustrate numerical examples to validate the betterment they provide in terms of Q-factor.

Acknowledgements

I express my profound gratitude to professor Shiva Kumar. Without his great insights and ideas this thesis would never be completed.

List abbreviations

ASE	Amplified Spontaneous Emission
BER	Bit Error Rate
CD	Chromatic Dispersion
CRC	Communications Research Centre
DBP	Digital Back Propagation
DCF	Dispersion-Compensating Fibers
DM	Dispersion Managed
DOF	Degree Of Freedom
DSP	Digital Signal Processing
DU	Dispersion Unmanaged
EDFA	Erbium-Doped Fiber Amplifiers
EMI	Electromagnetic Interference
FBG	Fiber Bragg Grating
FFT	Fast-Fourier Transform
FWM	Four-Wave Mixing
MMF	Multi-Mode Fiber
NLSE	Nonlinear *Schrödinger* Equation

NZ-DSF	Non-Zero Dispersion-Shifted Fiber
OPC	Optical Phase Conjugation
OFDM	Orthogonal Frequency Division Multiplexing
QAM	Quadrature Amplitude Modulation
PDF	Probability Density Function
PSK	Phase Shift Keying
SMF	Single-Mode Fiber
SOP	State Of Polarization
SPM	Self Phase Modulation
TF	Transmission Fiber
VDCF	Virtual Dispersion Compensating Fiber
WDM	Wavelength Division Multiplexing
XPM	Cross Phase Modulation

Contents

List of Figures

Chapter 1

Introduction and Problem Statement

1.1 Optical Fibers

The growing need for very high data rate has rendered electrical cable and copper wire based systems obsolete for long haul transmission system. Transmission capacity of copper can not satisfy our increasing demand for large bandwidths, since they operate in low frequency range and have high signal loss. Fiber optics (optical fibers) have proved to be the ideal transmission medium in this regard. Optical fibers are long, thin strands of very pure glass about the size of a human hair (Kumar and Deen, 2014). They are arranged in bundles called optical cables and used to transmit signals over long distances. Fiber optics introduced in the 1950's (Agrawal, 2012), which were very lossy. Optical fibers proposed to be used as a means of communication in early 1960's, but still the loss was too high. It has been proved that glass contaminants was causing that much loss (about 1000 dB/km), and could potentially be removed.

In 1970, new optical fibers manufactured had 20 dB/km loss and could be used for communication purposes. This improvement was significant, however, compared to coaxial cables, which had 5-10 dB/km loss, these fibers were still lossier, but their high transmission capacity were unique. Over a short period of time, researchers overcame this problem and developed optical fibers with 0.2 dB/km loss. Such a revolution coupled with the invention of Lasers in 1960's finally made a high capacity optical communication system possible (Sarkis, 2009).

1.2 Applications

Optical fibers are preferred over copper cables in systems that require high bandwidth, long distance or immunity to electromagnetic interference (EMI). There are numerous applications for optical fibers. Some but not all of them can be listed as below:

- Telecommunication purposes (Kumar and Deen, 2014),
- Medical applications (AlAmri *et al.*, 2016, Chapter 8),
- Fiber optic cable sensors (Dakin, 1988),
- Fiber optic Lasers (Okhotnikov, 2012),
- Military purposes (Benzoni and Orletsky, 1989).

1.3 Fiber Optic Communication Systems

Fiber optics revolutionized the world of telecommunication due to their extremely large bandwidth, low loss, resistance to EMI, their small size and light weight. They

can send several tera bits of information within a second ($\sim 10^{12} bps$). Nowadays, more than 80% of world long distance traffic is carried over fiber optics (Kumar and Deen, 2014). Therefore, fiber optic systems are the main backbone of today's communication systems worldwide, and it is of significant importance to get a thorough understanding of their characteristics and performance. Despite all the advantages we talked about, there are some drawbacks that put penalty on fiber optic systems capacity and realization. These characteristics, by either acting alone or interacting with each other, cause performance degradation which need to be dealt with. Many studies have been done around the world to overcome these issues and to reach the highest possible capacity of fiber optics. The following three fiber characteristics, are the main causes of the mentioned impairments in the current fiber optic systems.

1.3.1 Fiber Loss

Fiber loss is an important factor in optical communication systems, which limits its performance by reducing the signal power that reaches to the receiver. Due to this phenomena, fiber optic communication systems were limited to be used in short distance communications. researchers overcame this problem by inventing very pure silica glasses as well as optical amplifiers. Fiber losses depend on the wavelength of transmitted signal. The fiber cables used in today's communications, exhibit a loss of $0.2 dB/km$ in the wavelength region near $1.55 \mu m$. Material absorption and Rayleigh scattering, constitute the two main sources for fiber loss.

- **Material Absorption**

  Material absorption loss relates to the material used to create that fiber as well as its impurities. It can be divided into two categories, i.e., extrinsic absorption

and intrinsic absorption losses. Extrinsic absorption is due to the presence of imperfections in the atomic structure of the fiber material. To avoid this loss, we need to manufacture ultra pure silica fibers, which modern technology facilitates this fabrication. If there is no impurities and imperfections in the material, then entire absorption is due to intrinsic absorption. Intrinsic absorption relates to the vibration of atoms in the material used to make the fiber. Due to the interaction of these vibrations with the traveling signal, one or more wavelengths of light gets absorbed, hence this property can cause some amount of attenuation in the traveling signal.

- **Rayleigh Scattering**

  When a light wave is incident on a crystal, each atom emits a light wave of the same frequency (Kumar and Deen, 2014). When we have a perfect crystal that its molecules are spaced uniformly, the scattered light waves of all atoms add up destructively, so there is no scattered light. During the manufacturing process of optical fiber, usually there remains inhomogeneity in some regions, therefore, fiber can not be considered as a perfect crystal. Having this imperfection causes to the mentioned scattered light waves to not get canceled out, which results in signal loss in the fiber.

Propagating signals in the fiber exhibit an exponential reduction in their average power. In fact, propagation constant of the traveling wave, i.e., β in Eq. (1.1), is a complex number. The real part of β is proportional to the phase velocity of the mode produces a phase shift on propagation which changes rather rapidly with optical wavelength, and the imaginary part of β represents the loss (or gain) in the fiber and is a weak (but certainly not negligible) function of optical wavelength (Bass, 2001)

$$u(z) = u_0(z)\exp(j\beta z) \tag{1.1}$$

1.3.2 Dispersion

Dispersion occurs because of an inherent property in the medium that causes different spectral components of a wave to propagate at different speeds. This effect causes changes in the signal's temporal shape. In this case, dispersion causes a rearrangement of the signal spectral components in the time domain, resulting in temporal spreading of the information and eventually in severe distortion (Guenther, 2004). Dispersion introduces a fundamental limit to fiber communications and produces a signal distortion and intersymbol interference (in digital systems) which is unacceptable (Bass, 2001). There are multiple sources of dispersion that can be classified as

1. **Material Group Velocity Dispersion**

   Different frequencies of light in general interact at varying strengths with the fiber material which is specific to that medium, therefore causes dispersion.

2. **Waveguide Group Velocity Dispersion**

   Each waveguide has a specific geometry and dimensions, which cause different frequecy components act differently due to different boundary conditions at the core-cladding interface; this effect is called waveguide dispersion.

3. **Intermodal Dispersion**

   Multimode fibers can guide many different light modes due to their larger core size, and each mode travels with different velocity which causes dispersion. This

kind of dispersion is absent in single-mode fibers since they allow only one mode to propagate.

Dispersion Management

Material and waveguide dispersions are the main causes for chromatic dispersion (CD) in single-mode fibers. Since they have opposite signs with regard to each other, when they act together the total dispersion could become equal to zero in a specific wavelength. Beyond this wavelength, the fiber exhibits a region of anomalous dispersion. Dispersion acting alone on the signal will result in pulse broadening in both normal and nomalous dispersion regions, however, interaction of dispersion and nonlinearity can induce pulse compression in some cases as well (Kumar and Deen, 2014, Sec. 10.3). Anomalous dispersion has been used in the compression of pulses in optical fibers (Bass, 2001). Therefore, fibers acting in normal dispersion region cause pulse broadening and those acting in anomalous dispersion region cause pulse compression. Therefore, using these two regions and fiber properties, the dispersion problem can be managed in practice through a suitable dispersion-compensation scheme. There are different techniques to compensate for dispersion, and we will explain two of them briefly. For more information please refer to (Agrawal, 2011, Chapter 8).

- **Dispersion-Compensating Fibers:**

  Special dispersion-compensating fibers (DCFs) have been developed to be used as optical means to compensate for the dispersion, which provides an all-optical, fiber-based solution to the dispersion problem. Previously, it used to be done by optical filters, which were difficult to design (Agrawal, 2011).

- **Fiber Bragg Gratings:**

Fiber brag grating (FBG) is a periodic change of the fiber refractive index, formed from multiple layers of alternating materials with varying refractive index. They usually have a length of several millimeters to several centimeters with multiple disturbances of about a few 100 nm lengths each. The refractive index perturbation leads to the reflection of light propagating along the fiber in a narrow range of wavelengths. The range of wavelengths that are reflected is called the photonic stopband. Different kinds of FBGs have been developed since their first demonstration by Hill et al. in 1978 at the Canadian Communications Research Centre (CRC), Ottawa, Ont., Canada (Hill *et al.*, 1978)-(Kawasaki *et al.*, 1978). Constant period FBGs, apodized FBGs, and chirped FBGs, are some of the FBG types. Please refer to (Agrawal, 2011, Section 8.3) for more detailed information. Chirped fiber gratings were proposed for dispersion compensation as early as 1987. The chriped FBG causes varied delay for each frequency components, in which, low-frequency components of a pulse are delayed more because of increasing optical period (and the Bragg wavelength). FBGs cause no nonlinearity to the signal and have lower loss compared to DCFs.

1.3.3 Nonlinearity

An optical fiber medium is considered to be a nonlinear system. The nonlinear effects in optical fiber occur either due to intensity dependence of refractive index of the medium or due to Raman effects (Singh and Singh, 2007). The former effect is due to an existing phenomenon called Kerr effect which we will discuss in more details in the following, and the latter is not of our interest in this work, so we will ignore it. Kerr

effect is the most common nonlinear effect in optical fibers, and it is a change in the refractive index of a material due to an applied electric field. This means that as the optical intensity increases, the induced phase delay in the fiber gets larger (Kumar and Deen, 2014). Here, we refer to some consequences of the presence of Kerr effect in the optical systems.

1. **Self phase modulation (SPM):**

   One of the consequences of the Kerr effect is self-phase modulation (SPM). Since the change in refractive index due to the Kerr effect translates into a phase shift, the signal phase is modulated by its power distribution, which is known as SPM (Kumar and Deen, 2014). SPM is the most common nonlinear effect in single mode fibers.

2. **Cross phase modulation (XPM):**

   Cross phase modulation (XPM) occurs both in single wavelength channels, where there are stream of pulses traveling along the fiber, and interference happens between neighboring pulses which is called intra-channel XPM , and in wavelength division multiplexing (WDM) systems, in which they have multiple channels co-propagating through the fiber line, and the interaction between these channels cause phase shift on their signals, which is called inter-channel XPM. Therefore, The phase of a signal in a channel is modulated not only by its channel power (which causes SPM), but also by other channels, which is known as XPM (Kumar and Deen, 2014).

3. **Four-wave mixing (FWM):**

   Four-wave mixing (FWM) is a phenomenon in which interactions between two

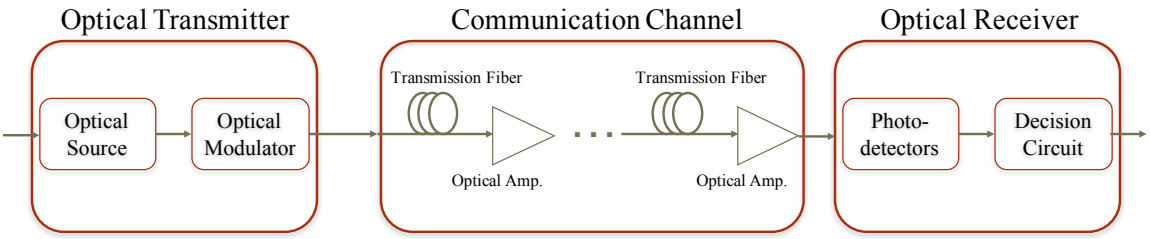

Figure 1.1: A fiber optic transmission system consists of three main blocks, namely, optical transmitters, communication channel, and optical receivers. Each of these blocks consist of different components.

or three wavelengths generates one or two new wavelengths. FWM acts as noise on channels (Kumar and Deen, 2014).

Although, fiber nonlinearities usually cause performance degradation and must be avoided in actual systems, they can be used to advantage in the generation of soliton for some applications (Bass, 2001). For more information about solitons please refer to (Mollenauer and Gordon, 2006).

1.4 Optical Components

As shown in Fig. 1.1, all fiber optic transmission systems include three main blocks, and each of those blocks have some sub-blocks.

1.4.1 Optical Transmitters

This block converts electrical data into an optical bit stream to transmit. It consists of

- **Optical source:** can be LED or Laser, which provides optical carrier,
- **Optical Modulator:** creates the optical bit stream.

1.4.2 Communication Channel

This block is responsible for transmitting optical bit streams generated by the optical transmitter. It consists of

- **Optical fibers:** fiber cables which have 0.2 dB/km loss and operate at 1550 nm region. Either single-mode fibers (SMFs), or multi-mode fibers (MMFs) can be used,
- **Optical amplifiers:** can be EDFA or Raman amplifiers. These amplifiers facilitate compensation for all the signal power loss throughout the line, without the need to optical to electrical and then electrical to optical conversions.

1.4.3 Optical Receivers

This block converts optical bit stream to the electrical data that was sent by the transmitter. It consists of

- **Photodetector:** converts light into electricity through the photoelectric effect,
- **Decision Circuit:** converts electrical time-varying signal into the original transmitted bit stream.

1.5 Literature Review

In this section, we will discuss about the history of three main concepts that are the focus of our work, i.e., coherent optical fiber communications, nonlinear phase noise, and dispersion managed (DM) systems.

1.5.1 A Brief History of Coherent Optical Fiber Communications

To transmit information through any channel, there are four degrees of freedom that we can use to modulate our signal, i.e., amplitude, phase, frequency, and polarization. Early optical communication systems used amplitude modulation of optical source at the transmitter, and intensity of the optical signal transmitted through an optical fiber was detected by a photodiode. This is known as amplitude-modulation and direct-detection scheme. Receivers base on direct-detection scheme were only sensitive to amplitude of the signal. Then, coherent receivers were developed in 1980's, (Okoshi and Kikuchi, 1980) and (Favre and D.LeGuen, 1980), which were sensitive to phase and polarization of the received signal. they used heterodyne detection for optical fiber communications. The use of coherent communication scheme was growing rapidly, and the motivation behind it was due to the high receiver sensitivity that enhanced the unrepeated transmission distance. Please refer to (Kikuchi, 2016) for more information.

The invention of erbium-doped fiber amplifiers (EDFAs) (Mears *et al.*, 1987), along with using wavelength-division multiplexing (WDM) techniques to increase the transmission capacity of a single fiber, put a temporary stop to further studies on coherent optical communications. Systems continued to employ EDFAs and WDM in amplitude modulation-direct detection shceme, until digital coherent receivers were introduced in 2005, (Tsukamoto *et al.*, 2005) and (McGhan *et al.*, 2005). These systems are still the most dominant systems used in practice. This is because digital coherent receiver enables to employ four-dimensional (4D) modulation formats, two degrees of freedom for the real and imaginary parts of the electric field amplitude, (or

equivalently, in-phase and quadrature (IQ) components), and two degrees of freedom for the state of polarization (SOP) (Kikuchi, 2011). In this thesis, we will use two polarizations, each with QAM-16 and QAM-256 modulation format.

1.5.2 A Brief History of Nonlinear Phase Noise

Amplified spontaneous emission (ASE) noise generated by optical amplifiers is the main noise source in fiber-optic communication systems, and can be adequately modeled as a Gaussian stochastic process (Demir, 2007). When ASE interacts with Kerr effect in fibers, it induces a nonlinear phase change to the optical signal leading to an unwanted stochastic phase shift. Fiber optic systems using phase shift keying (PSK) as their modulation scheme suffer greatly from this impairment. Phase shifts greater than a certain threshold, which can be different for various coding schemes, will lead to bit error (Kumar and Deen, 2014). Since this phase noise is stochastic in nature, there is no equalization technique that can compensate for it in digital domain. Gordon and Molleneuer first introduced this noise and derived an analytical expression for its variance (Gordon and Mollenauer, 1990). They pointed out that only two degrees of freedom (DOFs) of the noise modes are sufficient to describe the ASE noise added to the signal and the higher order noise modes play much less significant role if the optical bandwidth is not too large. These noise modes have the same form as the signal pulse. One of the noise modes is in phase with the signal and the other in quadrature. The in-phase component of the noise changes the amplitude of the signal pulse and, hence, leads to energy change while the quadrature component leads to a linear phase shift. The energy change is translated into an additional phase shift due to fiber nonlinearity (Kumar, 2009). Afterwards, taking into account higher

order noise modes, Mecozzi showed that if we use matched filter with its bandwidth equal to the signals bandwidth, two DOFs suffice to model the nonlinear phase noise; however, filters with larger bandwidth will require additional DOFs (Mecozzi, 1994). (Ho, 2003) and (Mecozzi, 2004) developed analytical expressions for the probability density function (PDF) of nonlinear phase noise. As for 2007, Demir has provided an extensive review about nonlinear phase noise in (Demir, 2007).

Many efforts have been done to compensate for nonlinear phase noise in different scenarios, some of which are as follows. Effect of nonlinear phase noise on the fiber-optic communication systems using M-ary PSK signals studied in (Ekanayake and Herath, 2013). Authors in (Xu *et al.*, 2014) developed a novel Viterbi-type adaptive maximum likelihood sequence detection algorithm considering both laser phase noise and nonlinear phase noise in coherent fiber-optic communication systems. An analytical formula for estimating the variance of nonlinear phase noise in coherent orthogonal frequency division multiplexing (OFDM) systems considering SPM, XPM and FWM has been developed in (Zhu and Kumar, 2010). An algorithm using soft-decision error-control code along side with the time correlation of the impairments due to nonlinearities has been proposed in (Pan *et al.*, 2015) to mitigate nonlinear phase noise, on a dual-polarization 16 QAM WDM system. (Wang *et al.*, 2015), developed a machine-learning based algorithm to mitigate nonlinear phase noise in an M-ary PSK-based coherent optical system.

1.5.3 A Brief History of DM systems

Gordon and Molleneuer ignored the effect of dispersion in their analysis, which later turned out to have a significant importance on phase noise. Many studies attempted

to consider the impact of dispersion on nonlinear phase noise. Kumar studied the nonlinear phase noise in optical fiber by taking the dispersion into account (Kumar, 2005)-(Kumar, 2009). He derived an analytical expression for the nonlinear phase noise variance using the first-order perturbation theory when DOFs=2 with Guassian pulse as the fiber input signal (Kumar, 2005), and later he extended his study to include arbitrary number of DOFs (Kumar, 2009). In (Kumar, 2005)-(Kumar, 2009), dispersion managed (DM) transmission system is analyzed. An DM system consists of two types of transmission fibers (TFs) within an amplifier spacing. Anomalous dispersion fiber for the first half and normal dispersion fiber for the second half, which compensates for the pulse broadening, due to the first half. (Almeida *et al.*, 2015) studiedx the optimum launch power for long haul optical fiber communication systems. Authors in (Weng *et al.*, 2018) have studied the OFDM systems using DM configuration using different segments of nonzero dispersion-shifted fiber (NZ-DSF) and DCF.

1.6 Thesis Overview

In this thesis we will study the effects of nonlinear phase noise in coherent fiber-optic systems. With the advent of coherent communication system, it is possible to compensate for pulse broadening in digital domain. Hence, the current trend is to have only one type of TF, and to compensate for pulse broadening due to the chromatic dispersion in digital domain using a dispersion compensating filter (DCF). Such a system is called dispersion unmanaged (DU) system.

Our results show that the variance of nonlinear phase noise reduces drastically as compared to the DM systems. This is because in DM systems, the system repeats

itself and nonlinear phase noise builds up coherently. However, in DU systems, pulses broaden monotonically and the nonlinear phase interaction between signal and ASE is different in different fiber spans. Hence, the contribution to nonlinear phase noise from various spans do not add up coherently, leading to lower nonlinear phase noise. These results include both analytical and numerical results which match quite well, when a single pulse, is transmitted over a long haul fiber optic link.

In the case of single pulse transmission, the variance of nonlinear phase noise decreases monotonically with dispersion on DU systems. The maximum achievable absolute dispersion, $|\beta_2|$, of the TF is limited to about $21ps^2/km$. So, we introduce additional dispersion by inserting FBGs immediately after the inline amplifiers. The dispersion of the FBG has the same sign as that of the TF. We have studied the performance for different symbol rates and find the optimum accumulated dispersion of FBG for each case. When the symbol rate is low, the FBG improves the performance significantly by lowering the nonlinear phase noise. However, at higher symbol rates, signal pulses broaden a lot, leading to interference with the neighboring pulses which could enhance the nonlinear phase noise. Hence, the amount of the required dispersion of FBG decreases as the symbol rate increases.

1.7 Outline

The rest of this thesis is organized as follows. In the chapter 2, we will discuss about the mathematical foundations of our study, and we will stress on the important techniques and assumptions that we have used throughout the thesis. Then, we will discuss about dispersion managed (DM) systems and we will explain the methods that has been used in the literature to derive the nonlinear phase noise variance. Chapter

3, includes dispersion unmanaged (DU) systems, and the derivation of nonlinear phase noise for this system model. In chapter 4, we will introduce fiber brag gratings (FBGs), and provide numerical examples to illustrate how they affect the system performance. In chapter 5, we will propose new system models, and prove that they reduce the nonlinear phase noise significantly, and we will validate it by various numerical examples. Chapter 6 will conclude this study.

Chapter 2

Theoretical Foundation and DM systems

2.1 Introduction

In this chapter we will give the mathematical background of our work, and then will discuss DM systems and the nonlinear phase noise variance derivation methods existing in the literature. We will first introduce the nonlinear *Schrödinger* equation (NLSE), which describes the propagation of the optical wave inside the optical fiber as a differential equation. Then, will explain how this equation should be solved analytically in different scenarios. Having all the parameters present in the NLSE makes it impossible to solve analytically, therefore, we will use split-step Fourier transform method as our numerical tool to solve it. Afterwards, we will talk about the DM systems and we will elaborate on the methods that has been used in the literature to derive the nonlinear phase noise variance as in (Kumar and Yang, 2005), (Kumar, 2005), and (Kumar, 2009).

2.2 Nonlinear *Schrödinger* Equation (NLSE)

Maxwell's equations (Griffiths, 2017) are the most effective tools to derive the wave propagation in every medium. Optical fiber is no exception, and if we convert the Maxwell's Equations cylindrical coordinates and use the appropriate boundary conditions of an optical fiber, it will yield the nonlinear *Schrödinger* equation (NLSE), which is the main differential equation to describe the wave propagation in fiber optics. Please refer to (Kumar and Deen, 2014, Chapter 10) for the derivation of NLSE. Here is the NLSE in the lossless form:

$$j\frac{\partial u(z,t)}{\partial z} - \frac{\beta_2(z)}{2}\frac{\partial^2 u(z,t)}{\partial t^2} = -\gamma \exp(-w(z))|u(z,t)|^2 u(z,t), \tag{2.1}$$

where γ is the nonlinear coefficient, the second-order derivative represents the dispersion, in which, β_2 is the dispersion coefficient, $w(z) = \int_0^z \alpha(s)ds$ is the fiber loss/amplifier gain profile, and $u(z,t)$ is the complex electric field of the traveling light wave.

NLSE models nonlinearity effects as SPM, XPM, FWM (see Sec. 1.3.3), optical solitons, and etc. The NLSE is a nonlinear partial differential equation that can not be solved analytically for arbitrary inputs. A numerical approach is therefore often necessary for an understanding of the nonlinear effects in optical fibers (Agrawal, 2012). Attempts have been made to introduce new methods of solving Eq. (2.1) numerically; among which, split-step Fourier method is the fastest in most cases compared with other techniques, and we will use it in our numerical simulations.

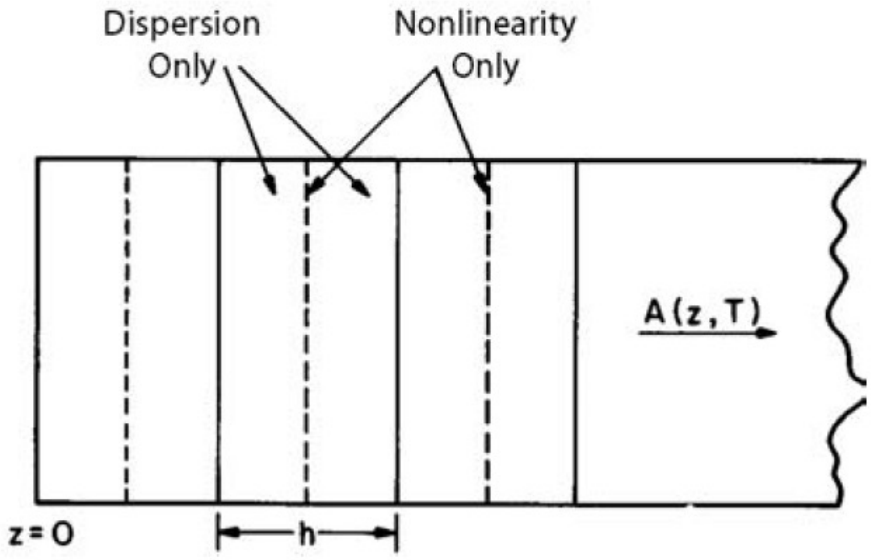

Figure 2.1: Schematic representation of split-step Fourier method, in which fiber length is divided into smaller segments of width h. $A(z,t)$ is the traveling wave (Agrawal, 2012).

2.2.1 Split-step Fourier transform method:

Split-step Fourier method is a pseudo-spectral numerical method that is used to solve nonlinear partial differential equations like NLSE. This method breaks the line into smaller splits and compute the solution for this split in each step, and also treats linear and nonlinear parts separately. In this method, linear step is solved in the frequency domain and the nonlinear step is solved in the time domain using fast-Fourier transform (FFT) method. Although, the dispersion and nonlinearity act simultaneously when pulse travels through the fiber, split-step Fourier method assumes that for small step sizes, we can apply the effect of each phenomenon separately as in Fig. 2.1, without loosing much accuracy. In this method, fiber length is divided into smaller segments of width h. From start to the middle plane of each segment only dispersion

has been included (solved in time domain), and in the middle plane, nonlinearity is included (by doing FFT first, including nonlinearity and then taking the inverse FFT), and then again only the dispersion has been taken into account (solved in the time domain, again) until the end of the segment. Depending on how exact we want the problem to get solved length h can be determined. As $h \to 0$, the results would be more accurate.

2.2.2 Gaussian Input:

As mentioned above, NLSE can not be solved analytically for arbitrary inputs, however, there are a few input pulses that make solving it possible. For example, using perturbation theory, NLSE can be solved analytically for Gaussian pulses. In what follows, we will calculate the propagating field envelope in the line, given that input signal is a Gaussian pulse.

First, suppose that the fiber is linear, which enables us to use fiber transfer function (Kumar and Deen, 2014, Sec. 2.5), i.e.,

$$H_f(\omega, z) = \exp(-\frac{\alpha z}{2} + j\beta_1 \omega z + \frac{j\beta_2 \omega^2 z}{2}), \tag{2.2}$$

The following summarizes the steps to calculate the output a single-mode optical fiber for a given input signal, when the fiber is supposed to be linear, (Kumar and Deen, 2014, Sec. 2.5):

- Take the Fourier transform of the input signal,
- Multiply it by the fiber transfer function in Eq. (2.2),
- Take the inverse Fourier transform.

The input pulse is

$$u_{in}(0,t) = \sqrt{E}F(t), \tag{2.3}$$

$$F(t) = \frac{\sqrt{P}}{T_0}\exp\left(-\frac{t^2}{2T_0^2}\right), \tag{2.4}$$

where P is the peak power, T_0 is the half-width at $1/e$- intensity point. $F(t)$ is normalized, i.e., its energy is unity, therefore, energy of the pulse is E. The peak power P, and energy E, are related by

$$P = \frac{E}{\sqrt{\pi}T_0}. \tag{2.5}$$

Having Eq. (2.3) as the fiber input, and following the mentioned steps, pulse evolution can be described as

$$u_{lin}(z,t) = \sqrt{E}F(z,t), \tag{2.6}$$

$$F(z,t) = \frac{\sqrt{P}T_0}{T(z)}\exp\left(-\frac{t^2}{2T^2(z)}\right), \tag{2.7}$$

where

$$T^2(z) = T_0^2 - jS(z), \tag{2.8}$$

$$S(z) = \int_0^z \beta_2(s)ds, \tag{2.9}$$

where $F(z,t)$ is normalized, and $S(z)$ is the accumulated dispersion to the point z.

2.2.3 Perturbation Theory

Eq. (2.6) gives the linear description of the propagating field envelope in the fiber. However, optical fiber is nonlinear medium and the impact of the nonlinearity on the evolution of pulse should be taken into account. As mentioned previously, there is no way to exactly solve the NLSE in general, unless we use some approximations. Therefore, we need to develop an appropriate tool to deal with this problem. One method that is called perturbation theory can be used in these cases. Perturbation theory breaks the problem into a dominant part (linear part of the propagating field in our case) and an unsolvable (perturbed) part. The perturbed part in general, is a small deformation of the dominant part. Throughout our study, we will use perturbation theory to calculate the fields at each point in the line.

$$u(z,t) = u_0(z,t) + \gamma u_1(z,t) + \gamma^2 u_2(z,t) + \gamma^3 u_3(z,t) + \ldots, \tag{2.10}$$

In Eq. (2.10), $u(z,t)$ on the right hand side, is the propagating signal throughout the fiber, $u_0(z,t)$ on the left hand side, is the linear part of $u(z,t)$, which is solvable as in Eq. (2.6), and the remaining terms determine the nonlinearity of $u(z,t)$, that are considered as small deformation of $u_0(z,t)$. Depending of how nonlinear the signal is, the order of the perturbation is chosen. Usually, for the range of practical launch powers, it is sufficient to use only first order perturbation theory to correctly model the signal as in (Kumar, 2005) and (Kumar, 2009), however, in some applications, second order perturbation theory is needed (Kumar and Yang, 2005). We will also assume that our system is quasi-linear, i.e. the nonlinearity is considered as a small perturbation to the main system, which is linear. So, the signal traveling in the line will consist of a linear part and the small nonlinear correction, therefore, we use the

first order correction to the optical field envelope, i.e.,

$$u(z,t) = u_0(z,t) + \gamma u_1(z,t). \tag{2.11}$$

Substituting Eq. (2.11) in Eq. (2.1), we will get:

$$j\frac{\partial u_1(z,t)}{\partial z} - \frac{\beta_2}{2}\frac{\partial^2 u_1(z,t)}{\partial t^2} = -\gamma \exp(-w(z))|u_0(z,t)|^2 u_0(z,t). \tag{2.12}$$

Using Eq. 2.12, we can calculate the perturbed signal $u_1(z,t)$, when the input signal $u_0(z,t)$ is a Gaussian pulse. In order to avoid repetition, we will calculate $u_1(z,t)$ for our system in chapter 3.

Up to now we have considered the signal going through the fiber without taking the effects of fiber-optic systems devices, which are used in practical systems, into account. Amplifiers, for example, are essential components in long haul systems, and they have enabled us to transmit information to a very long distance with a very low error rate. Despite all the benefits they brought up to the fiber optic systems, they also add noise to the line, which causes both linear and nonlinear impairments to the received signal, called linear phase noise and nonlinear phase noise, respectively (please see Secs. 1.3.3 and 1.5.2). In the next section, we will study DM systems (see Sec. 1.5.3). There have been many works on this DM systems, however, to avoid longevity, we only study the derivation of nonlinear phase noise as in (Kumar, 2005), that later expanded in (Kumar, 2009), which is relates the most to our study.

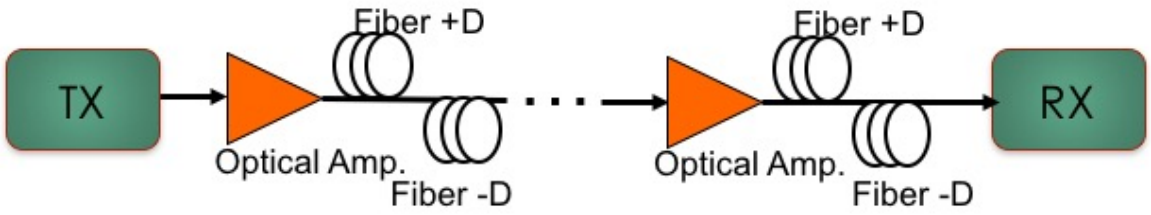

Figure 2.2: Dispersion managed (DM) system, block diagram representation. Dispersion and loss are totally compensated immediately after the next amplifier.

2.3 Dispersion Managed (DM) Systems

Consider an amplified transmission system as in Fig. 2.2. Transmitter sends the signal, due to loss in the line, EDFAs exactly compensates for the power loss. The spacing between amplifiers (which we assume it is $80km$) has been divided into two segments of equal length ($40km$ for each segment), first half has positive dispersion parameter ($+D$), so signal gets broadened as it propagates down the fiber, and the second half has negative dispersion parameter ($-D$), which means the broadened signal, will compress throughout that segment, and will compensate for all of the broadening happened in the first half. NLSE in Eq. (2.1), turns into Eq. (2.13) in amplified transmission system as below

$$j\frac{\partial u(z,t)}{\partial z} - \frac{\beta_2(z)}{2}\frac{\partial^2 u(z,t)}{\partial t^2} = -\gamma \exp(-w(z))|u(z,t)|^2 u(z,t) + jR(z,t), \qquad (2.13)$$

where R is the noise field added by the amplifier.

$$R(z,t) = \sum_{m=1}^{N_a} \delta(z - L_m) n^{(m)}(t), \qquad (2.14)$$

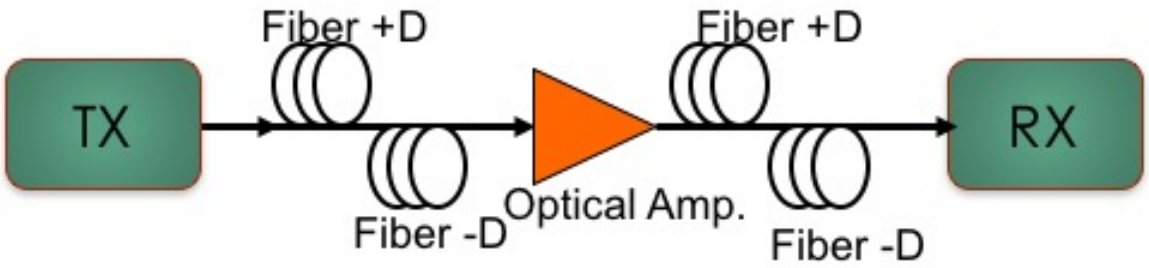

Figure 2.3: Transmission system with only one EDFA. Nonlinearity has been ignored before the amplifier.

where L_m is the location of an amplifier, and $n^{(m)}(t)$ is the noise field due to an amplifier located at L_m. The mean and autocorrelation function of the noise field are given by:

$$< n^{(m)}(t) >= 0, \tag{2.15}$$

$$< n^{(m)}(t)n^{(m)*}(t') >= \rho_m \delta(t - t'), \tag{2.16}$$

$$< n^{(m)}(t)n^{(m)}(t') >= 0, \tag{2.17}$$

where ρ_m is the ASE power spectral density per polarization of an amplifier located at L_m, given by (Gordon and Mollenauer, 1990)

$$\rho_m = n_{sp} h \bar{v} (G_m - 1), \tag{2.18}$$

where G_m is the gain of the amplifier, n_{sp} is spontaneous noise factor, h is Plancks constant and $\bar{v}$ is the mean optical carrier frequency. There can be multiple amplifiers in the line depending on the total length of the transmission system. Since, the statistical characteristics of each EDFA is independent of the other EDFAs, to calculate the variance of the nonlinear phase noise, each EDFA can be considered separately,

so, in (Kumar, 2009), the variance of the phase noise added by each EDFA has been calculated, and added altogether as the overall nonlinear phase noise variance. Therefore, lets consider a system with only one EDFA, as in Fig. 2.3. The nonlinearity before the EDFA has been ignored, so the transmission system before the amplifier is linear and the field envelope can be calculated as in Eq. (2.7) of Sec. 2.2.2. We ignore the mathematical calculation of the phase noise variance in this section for brevity, because we will discuss it in detail in chapter 3, when studying our own system setup. Please refer to (Kumar, 2009) for phase noise variance derivation for the system in Fig. 2.2.

The output phase at the receiver in the system shown in Fig. 2.2 is

$$\phi \approx \gamma E g_{fr}(L_m) + \gamma \delta E g_{fr}(L_m) + \frac{n_{0i}}{\sqrt{E}}, \tag{2.19}$$

where L_m is the position of the mth amplifier, $g_{fr}(L_m) = Re[g_f(L_m)]$, and

$$\delta E = 2\sqrt{E} n_{0r}, \tag{2.20}$$

$$g_f(L_m) = \frac{T_0}{\sqrt{\pi}} \int_{L_m}^{L_{tot}} G(r) dr, \tag{2.21}$$

where L_{tot} is the total length of the transmission system, and

$$G(r) = \frac{\exp[-w(r)]}{\sqrt{[1 + T_0^2 \Delta(r)][T_0^4 + 3S^2(r) + 2jT_0^2 S(r)]}}, \tag{2.22}$$

$$\Delta(r) = \frac{T_0^2 - jS(r)}{T_0^2[T_0^2 + j3S(r)]}, \tag{2.23}$$

where $S(z)$ is defined in Eq. 2.9, and T_0 is the half-width at $1/e$- intensity point.

Terms proportional to γ^2, n_{0r}^2, n_{0i}^2 and $n_{0r}n_{0i}$, are ignored due to their insignificant contributions. First term in Eq. (2.19) represents the deterministic nonlinear phase change, which can be removed in digital domain by digital back propagation (DBP). Therefore, what remains, is the non-deterministic terms, which are called nonlinear phase noise (2nd term in Eq. 2.9), and linear phase noise (3rd term in Eq. 2.9). There is no equalization technique to remove these two impairments, due to their stochastic nature. The best way to tackle this problem is to minimize the their variance. Therefore, the phase changes due to ASE of the amplifier located at L_m are

$$\delta\phi_m = \gamma\delta E g_{fr}(L_m) + \frac{n_{0i}}{\sqrt{E}}, \tag{2.24}$$

Using Eqs. (2.16), (2.17), and Eq. (2.20) we find

$$< n_{0r}^2 >=< n_{0i}^2 >= \frac{\rho_m}{2}, \tag{2.25}$$

$$< \delta E^2 >= 2\rho_m E. \tag{2.26}$$

Therefore, we obtain

$$< \delta\phi_m^2 >= 2\rho_m E[\gamma g_{fr}(L_m)]^2 + \frac{\rho_m}{2E}, \tag{2.27}$$

The first and the second terms on the right hand side of the Eq. (2.27) represent the variance of nonlinear phase noise and linear phase noise, respectively, due to the amplifier located at L_m.

Total phase noise variance is the sum of the variances due to each amplifier, as

given by Eq. (2.27)

$$< \delta\phi^2 >= \sum_{m=1}^{N_a} < \delta\phi_m^2 >, \tag{2.28}$$

$$< \delta\phi^2 >= \frac{N_a(N_a-1)(2N_a-1)\rho E(\gamma h_{fr})^2}{3} + \frac{\rho N_a}{2E}, \tag{2.29}$$

where N_a is the number of EDFAs in the line. Please refer to (Kumar, 2009) for the detailed derivation. Eq. (2.29) shows that there should be an optimal E, and therefore optimal launch power P, that gives the minimum phase noise variance. differentiating $< \delta\phi^2 >$ with respect to E and setting it to zero, and then using $P = \frac{E}{\sqrt{\pi}T_0}$, will give (Kumar, 2009)

$$P_{opt} = \frac{1}{\gamma h_{fr}\sqrt{\pi}T_0}\sqrt{\frac{3}{2(N_a-1)(2N_a-1)}}. \tag{2.30}$$

As it can be seen in Eq. (2.29), the nonlinear phase noise variance (the first term on the right hand side) becomes dominant for long haul systems, as it increases cubically with the number of EDFAs.

In the next chapter we will discuss dispersion unmanaged (DU) systems, derive its phase noise variance, and compare it to the results of DM systems shown in here through some numerical simulations.

Chapter 3

Dispersion Unmanaged (DU) Systems

3.1 Introduction

With the advent of coherent receivers, we were able to use multi-dimensional modulation formats in our transmission systems, such as PSK and QAM. In these systems, the change in the phase of the recieved siganal can cause error when detecting the signal. As discussed in the previous chapter, nonlinear phase noise is one of the main sources that causes malicious effects in the fiber optic systems at high launch powers. In this chapter, we stress that, managing the dispersion has a significant impact on this effect, and we use the system model called dispersion unmanaged (DU) system.

We derive an analytical expression for the linear and nonlinear phase noise variance in DU fiber optic systems using a first-order perturbation theory. Then, we provide numerical examples to illustrate the behavior of the developed phase noise variance in terms of dispersion and distance. The results show that in dispersion unmanaged

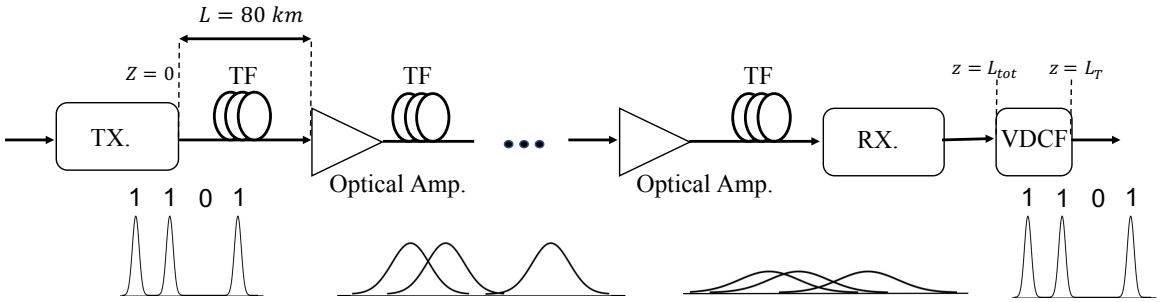

Figure 3.1: Fiber-optic system setup. There is no dispersion compensation within the line. VDCF = virtual dispersion compensating fiber, TF = transmission fiber. $L_T = L_{tot} + L_{VDCF}$, $L_{tot} = N_a L$, N_a is the number of amplifiers, and $L = 80\ km$.

systems nonlinear phase noise interaction between the amplified spontaneous emission and the signal does not grow as much as in dispersion managed systems, because this interaction is different in each fiber-amplifier span, so the system does not repeat itself. Therefore, the nonlinear phase variance in a dispersion unmanaged system is much lower than the corresponding noise variance in a dispersion managed system.

3.2 System Setup

In this chapter, we use the system configuration as shown in Fig. 3.1. We excite a Gaussian pulse as the input signal with peak power P. Due to the attenuation in the fiber we use erbium doped fiber amplifiers (EDFAs) in the line to exactly compensate for it; however, they add ASE noise to the system. We assume that the the mean noise power added by the amplifiers is much lower than the input signal power P. We use EDFAs every 80 km. We assume that our system is quasi-linear, i.e. the nonlinearity is considered as a small perturbation to the main system, which is linear.

We do not manage the dispersion throughout the line and allow the signal to keep

broadening to the end of the line, and then we compensate the dispersion for the whole line in digital domain.

3.3 Nonlinear Phase Noise

The propagation of an electric field envelope in the optical fiber obeys the nonlinear *Schrödinger* equation (NLSE) in the lossless form shown in Eq. (2.13). $R(z,t)$ is defined in Eq. (2.14), and statistical properties of the noise is as Eqs. (2.15)-(2.17). Using a Gaussian pulse at the fiber input in the Eq. (2.13), and ignoring the amplifier noise and nonlinearity in the fiber, the pulse evolution can be described as Eq. (2.6), i.e.,

$$u_{lin}(z,t) = \sqrt{E}F(z,t), \tag{3.1}$$

$$F(z,t) = \frac{\sqrt{P}T_0}{T(z)} \exp\left(-\frac{t^2}{2T^2(z)}\right), \tag{3.2}$$

where

$$T^2(z) = T_0^2 - jS(z), \tag{3.3}$$

$$S(z) = \int_0^z \beta_2(s)ds, \tag{3.4}$$

where $F(z,t)$ is normalized, and $S(z)$ is the accumulated dispersion to the point z.

Including nonlinear effects throughout the fiber in our model will change our method of solving Eq. (2.13), for which we use perturbation theory to do that. In this chapter, we use the first order correction to the optical field envelope defined in Eq. (2.11),

$$u(z,t) = u_0(z,t) + \gamma u_1(z,t). \tag{3.5}$$

where $u_0(z,t)$ is the linear field in the absence of noise, it is given by (3.1), and $u_1(z,t)$ is the first order perturbation due to nonlinear effects. Substituting (3.5) in (2.13) (without the amplifier noise term) and collecting the terms proportional to γ, we obtain:

$$j\frac{\partial u_1(z,t)}{\partial z} - \frac{\beta_2}{2}\frac{\partial^2 u_1(z,t)}{\partial t^2} = -\gamma \exp(-w(z))|u_0(z,t)|^2 u_0(z,t), \quad z > L_m. \tag{3.6}$$

Eq. (3.6) will help us obtain the nonlinear component of the field envelope ($u_1(z,t)$) through the fiber. In the following, we first determine the linear part of the electrical field for all over the line, and then derive the nonlinear part. We have EDFAs spaced 80 km apart, as shown in Fig. 3.1. Since the noise of these amplifiers are statistically independent, we can find the variance for each of them separately and then add them altogether. So we may consider a line with only one amplifier located at L_m to derive $u_1(z,t)$.

3.3.1 The Linear Field

The linear part of the field envelope before and after the amplifier located at L_m (without considering the amplifier noise) can be described by ((3.1)-(3.4)):

$$u_0(z,t) = \sqrt{E}F(z,t) = \frac{\sqrt{P}T_0}{T_1(z)} \exp\left(-\frac{t^2}{2T_1^2(z)}\right). \; z \leq L_m, \tag{3.7}$$

$$u_0(z,t) = \sqrt{E}F(z,t) = \frac{\sqrt{P}T_0}{T_2(z)} \exp\left(-\frac{t^2}{2T_2^2(z)}\right), \; z \geq L_m \tag{3.8}$$

where

$$T_1^2(z) = T_0^2 - jS_m(z), \quad S_m(z) = \int_0^z \beta_2(s)ds, \ z \leq L_m, \tag{3.9}$$

$$T_2^2(z) = T_1^2(L_m) - jS(z), \quad S(z) = \int_{L_m}^z \beta_2(s)ds, \ z \geq L_m. \tag{3.10}$$

The linear part immediately after the mth amplifier is:

$$u_0(L_{m+}, t) = u_0(L_{m-}, t) + n^{(m)}(t) \tag{3.11}$$

$n^{(m)}(t)$ has the statistics given by (2.15)-(2.17). We will use $n(t)$ instead of $n^{(m)}(t)$ for simplicity. We assume two DOFs for the noise, and represent them by the Gaussian base function $F(z,t)$. So we have:

$$n(t) = n_0 F(L_m, t), \tag{3.12}$$

where $n_0 = n_{0r} + jn_{0i}$, where n_{0r} and n_{0i} are the amplitudes of the in-phase component and quadrature components of the noise field, respectively. n_0 is a random variable and $n(t)$ is a random process. Due to our assumption of two DOFs, the random process can be approximated as the superposition of two noise modes that have the same temporal shape as the signal and the amplitude n_0 being a random variable. Using (3.8) and (3.12) in (3.11), we find

$$u_0(L_{m+}, t) = (\sqrt{E} + n_0)F(L_m, t), \tag{3.13}$$

Considering (3.13) as the input for the line at $z = L_m$, the linear part of the optical field envelope for $z > L_m$ can be described as

$$u_0(z,t) = (\sqrt{E} + n_0)F(z,t), \quad z > L_m \tag{3.14}$$

The virtual dispersion compensating fiber (VDCF) introduced in the digital signal processing (DSP) will compensate for all the dispersion that has broadened our signal, so the linear component after the VDCF is

$$u_0(L_T,t) = (\sqrt{E} + n_0)F(0,t), \tag{3.15}$$

where $L_T = L_{tot} + L_{VDCF}$, $L_{tot} = N_a L$, N_a is the number of amplifiers and L is the distance between each amplifier spacing i.e. 80 km in our model, and L_{VDCF} is the length of the VDCF at the end of the line. We assume that the VDCF is linear, i.e. its $\gamma = 0$.

3.3.2 The Nonlinear Field

We will use (3.13) as our input for (3.6) to obtain $u_1(z,t),\ z > L_m$. So Eq. (3.8) is modified as

$$u_0(z,t) = \sqrt{\frac{T_0}{\sqrt{\pi}}} \frac{(\sqrt{E} + n_0)}{T_2(z)} \exp\left(-\frac{t^2}{2T_2^2(z)}\right). \tag{3.16}$$

We use (3.16) to evaluate the right hand side of (3.6)

$$|u_0(z,t)|^2 u_0(z,t) = c(z) \exp\left(-R(z)t^2\right), \tag{3.17}$$

where

$$c(z) = \left(\frac{T_0}{\sqrt{\pi}}\right)^{\frac{3}{2}} \frac{(\sqrt{E}+n_0)(E+\delta E)}{T_2(z)|T_2(z)|^2}, \tag{3.18}$$

$$R(z) = \left(\frac{T_0^2}{|T_1(L_m)|^4 + 2S_m(L_m)S(z) + S^2(z)} + \frac{1}{2T_2^2(z)}\right), \tag{3.19}$$

$$\delta E = 2\sqrt{E}n_{0r}. \tag{3.20}$$

Taking the Fourier transform of Eq. (3.6), we find

$$j\frac{\partial \tilde{u}_1(z,\omega)}{\partial z} + \alpha(z)\tilde{u}_1(z,\omega) = -p(z,\omega), \quad z > L_m, \tag{3.21}$$

where

$$\alpha(z,\omega) = \frac{\beta_2(z)\omega^2}{2}, \tag{3.22}$$

$$p(z,\omega) = \gamma \exp(-w(z))\mathcal{F}\left(|u_0(z,\omega)|^2 u_0(z,\omega)\right). \tag{3.23}$$

Using (3.17), we have

$$\mathcal{F}\left(|u_0(z,\omega)|^2 u_0(z,\omega)\right) = c(z)\sqrt{\frac{\pi}{R(z)}}\exp\left(-\frac{\omega^2}{4R(z)}\right). \tag{3.24}$$

Solving the first-order differential equation (3.21) yields

$$\tilde{u}_1(z,\omega) = j\int_{L_m}^{z} \exp\left(j\frac{1}{2}\omega^2(S(z)-S(y))\right)p(y)dy. \tag{3.25}$$

Substituting Eqs. (3.23) and (3.24) in (3.25), and setting $z = L_T$, we find

$$\tilde{u}_1(L_T,\omega) = j\int_{L_m}^{L_T} \gamma \exp(-w(y))c(y)\sqrt{\frac{\pi}{R(y)}} \times \exp\left[-\left(\frac{1}{4R(y)} - j\frac{1}{2}(S(L_T)-S(y))\right)\omega^2\right]dy, \tag{3.26}$$

Taking the inverse Fourier transform of (3.26) gives us the nonlinear part of the propagating field

$$u_1(L_T,t) = j\int_{L_m}^{L_T} A(L_T,y)\exp\left(\Delta(y)t^2\right)dy, \tag{3.27}$$

where

$$A(L_T,y) = \frac{\gamma\exp(-w(y))c(y)}{\sqrt{1-j2R(y)(S(L_T)-S(y))}}, \tag{3.28}$$

$$\Delta(y) = \frac{R(y)}{1-j2R(y)(S(L_T)-S(y))}. \tag{3.29}$$

Appendix A includes the derivation of Eq. (3.27). Using (3.27) and (3.15) in (3.5), we have

$$u(L_T,t) = (n_0+\sqrt{E})F(0,t)\times\left[1+j\sqrt{\frac{E}{P}}\int_{L_m}^{L_T}\frac{A(L_T,y)}{\sqrt{E}+n_0}\exp\left(-\left(\Delta(y)-\frac{1}{2T_0^2}\right)t^2\right)dy\right]. \tag{3.30}$$

It is worthwhile to note that setting $S(L_T)=0$ in Eq. (3.30), which is technically equivalent to compensating the dispersion as in DM systems, will lead to the result of (Kumar, 2009, Equation (21)).

3.3.3 Matched Filter

We use a matched filter at the receiver to cancel out the higher-order noise components, since they are orthogonal to our input signals (Kumar and Deen, 2014), so the receiver makes the decision based on the matched filter's output.

$$u_f = \int_{-T_b/2}^{+T_b/2} u(L_T,t)F^{\star}(0,t)dt \approx \int_{-\infty}^{+\infty} u(L_T,t)F^{\star}(0,t)dt, \tag{3.31}$$

where T_b is the bit interval. Substituting (3.2) and (3.30) in (3.31), we find

$$u_f = (n_0 + \sqrt{E})\left[1 + j(E + \delta E) g_{fm}(L_T)\right], \tag{3.32}$$

where

$$g_{fm}(L_T) = \frac{T_0}{\sqrt{\pi}} \times \int_{L_m}^{L_T} \frac{T_0 \gamma \exp(-w(y))\sqrt{2}}{T_2(y)|T_2(y)|^2 \sqrt{(1 - j2R(y)(S(L_T) - S(y)))\,(1 + 2T_0^2\Delta(y))}} dy. \tag{3.33}$$

The detailed derivation of Eq. (3.32) can be found in Appendix B.

3.3.4 Phase Noise and Its Variance

The phase of the filter output can be calculated as:

$$\phi_m = \tan^{-1}\frac{Im(u_f)}{Re(u_f)} \approx \frac{n_{0i}}{\sqrt{E}} + E g_{fr_m}(L_T) + 2\sqrt{E} n_{0r} g_{fr_m}(L_T), \tag{3.34}$$

where $E g_{fr_m}(L_T) = E Re[g_{f_m}(L_T)]$ is the deterministic nonlinear phase change in the absence of ASE. In (3.34), we have ignored terms proportional to γ^2, n_{0r}^2, n_{0i}^2 and $n_{0r} n_{0i}$. The phase change due to the ASE of the amplifier can be shown as

$$\delta\phi_m \simeq \frac{n_{0i}}{\sqrt{E}} + 2\sqrt{E} n_{0r} g_{fr_m}(L_T), \tag{3.35}$$

Variance of the phase noise in (3.35) can be calculated as:

$$< \delta\phi_m^2 > \simeq \frac{1}{E} < n_{0i}^2 > + 4E < n_{0i}^2 > \left(g_{fr_m}(L_T)\right)^2. \tag{3.36}$$

Using Eqs. (2.15)-(2.16) and (3.20), we find

$$< n_{0r}^2 >=< n_{0i}^2 >= \frac{\rho_m}{2}, \tag{3.37}$$

$$< \delta E^2 >= 2\rho_m E. \tag{3.38}$$

With the help of (3.37)-(3.38), (3.36) may be rewritten as

$$< \delta\phi_m^2 >\simeq \frac{\rho_m}{2E} + 2E\rho_m \left(g_{fr_m}(L_T)\right)^2, \tag{3.39}$$

Therefore

$$< \delta\phi^2 >= \sum_{m=1}^{N_a} < \delta\phi_m^2 >, \tag{3.40}$$

Eq. (3.39) is the main result of this chapter.

3.4 Simulation Results and Discussion

In this section, using some numerical examples, we examine the nonlinear phase noise variance obtained in (3.39) and illustrate how it depends on distance as well as dispersion parameter D. Also, we will compare the nonlinear phase noise in DM system in (Kumar, 2009) with DU system studied in this chapter. We have used split-step Fourier transform to simulate the propagation in optical fibers numerically, and compared it with our analytical calculation derived in Eq. (3.39).

We assume the following parameters throughout this chapter: $\gamma = 2.43\, W^{-1}km^{-1}$, $\alpha = 0.2\ dB/km$, bit rate $= 40\ Gb/s$, $n_{sp} = 1$, $T_0 = 7.5$ ps, and amplifier spacing is 80 km. We use transmission fiber with anomalous dispersion between inline amplifiers.

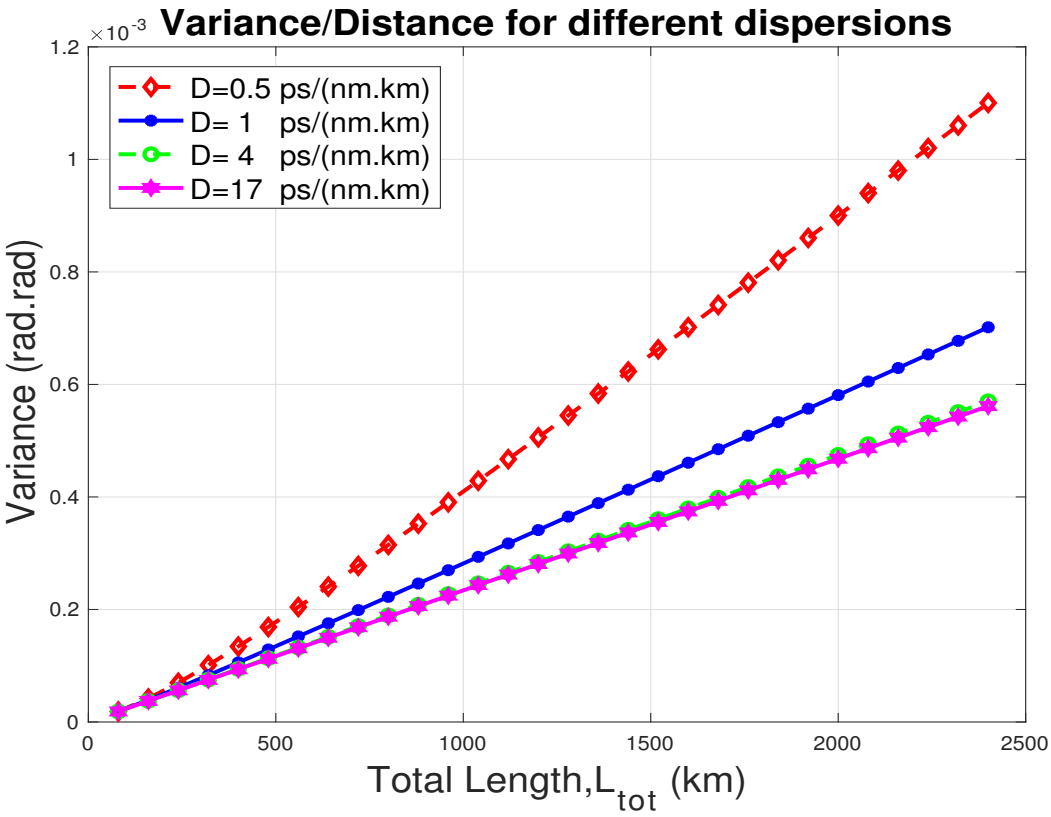

Figure 3.2: Phase noise variance in terms of distance for different values of dispersion parameter, with $P = 10mW$

Figure 3.2 shows how the phase noise variance changes with distance. We can see that with signal propagating through the fiber line, the variance keeps increasing, which can be directly deduced from the self phase modulation (SPM) acting on that signal - the longer the signal propagates in the fiber, the more change the fiber nonlinearity adds to its phase. However, SPM acting alone in the absence of ASE is the deterministic nonlinear phase change (second term in (3.34)) which can be removed by the digital equalizers. It is the interaction of SPM and ASE leading to stochastic change in phase (third term in (3.34)), that can not be compensated by equalizers and expected to set the limit on channel capacity.

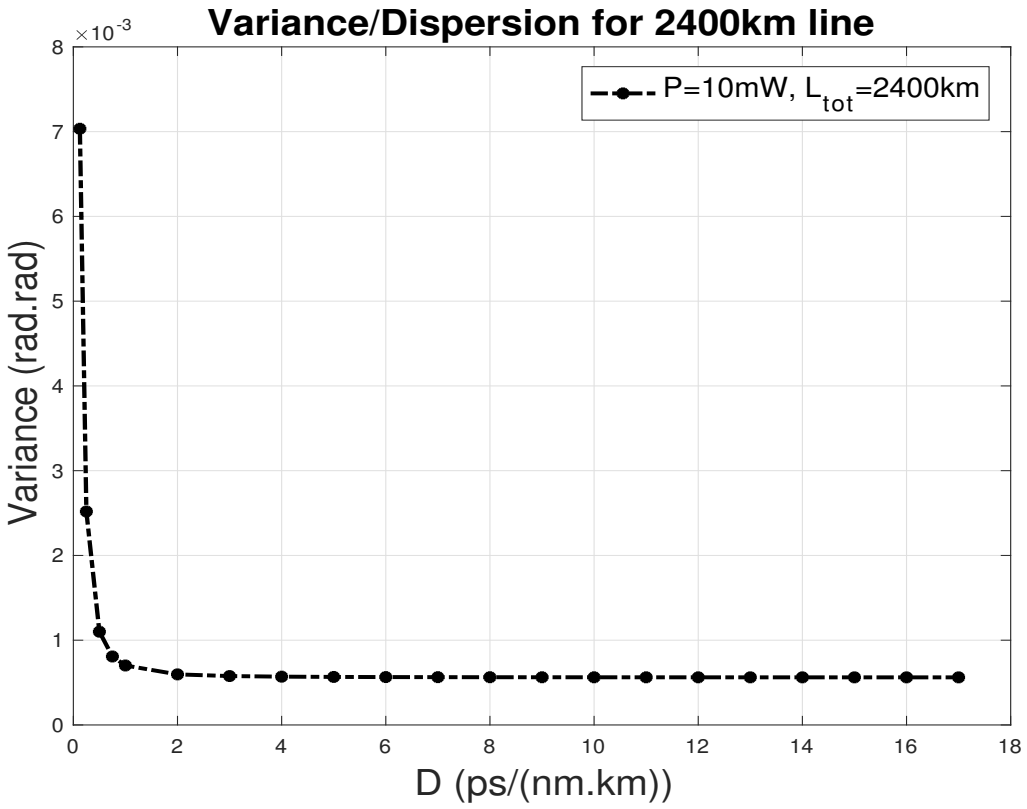

Figure 3.3: Phase noise variance in terms of dispersion parameter, with $P = 10mW$ and $L_{tot} = 2400km$

Having no dispersion in the fiber will cause the ASE noise to resonate, which will increase its variance dramatically. Therefore, introducing small amount of dispersion will reduce it as we can see for $D = 0.5$ ps/(nm.km) in Fig. 3.2. The more we increase the dispersion, the smaller variance we get, however, as it can be seen in this figure, the improvement from $D = 4$ ps/(nm.km) to $D = 17$ ps/(nm.km), which is the approximate dispersion parameter of a standard single mode fiber, is negligible. Fig. 3.3 illustrates this phenomena for fiber line length of $L_{tot} = 2400$ km. It can be seen that, when the dispersion parameter is very small, a tiny increase in it will reduce the variance drastically. At larger dispersions, the change in variance is negligible, since

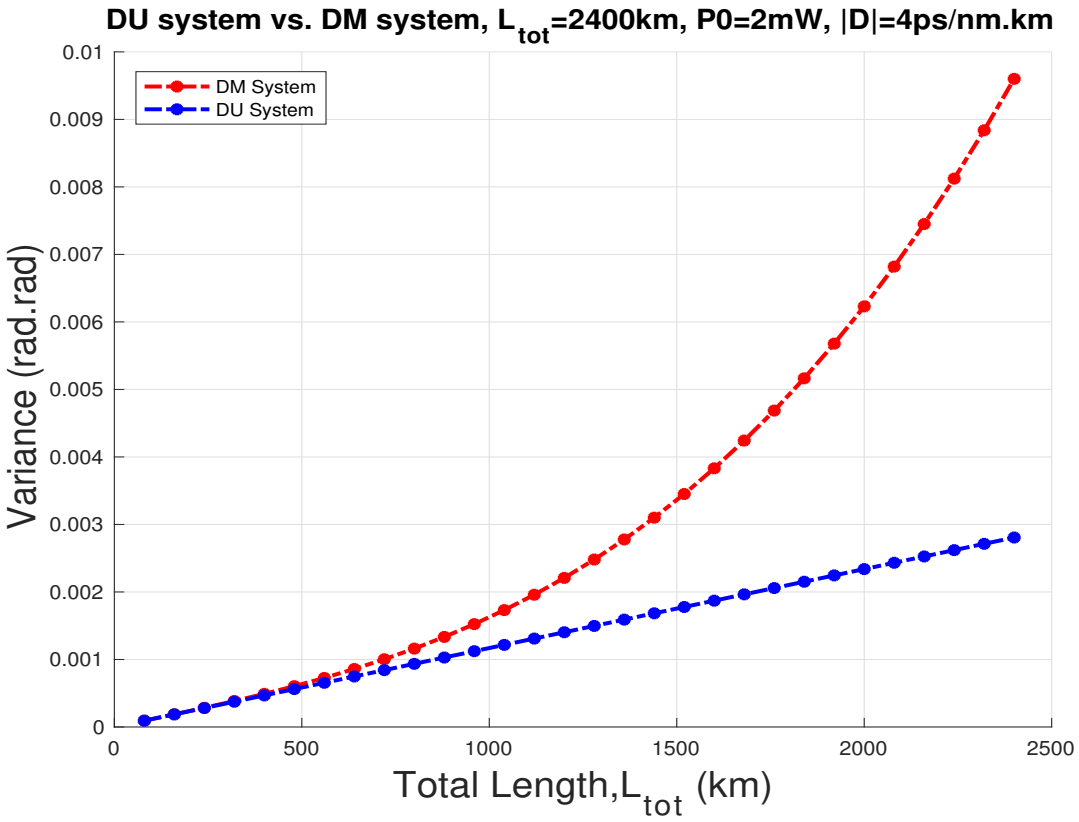

Figure 3.4: Nonlinear phase noise variance of DU system and DM system are compared, with $P = 2mW$, $L_{tot} = 2400km$, and $|D| = 4ps/nm.km$

the dominant contribution to the variance arises from linear phase noise, rather than nonlinear phase noise. To get a better sense of these values, it is good to note that, typical dispersion parameters of deployed non-zero dispersion-shifted fiber (NZDSF) is in the range of 4 $ps/nm/km$ to 7 $ps/nm/km$, that of dispersion-shifted fiber (DSF) is in the range of 0.25 $ps/nm/km$ to 1 $ps/nm/km$.

Fig. 3.4, compares the nonlinear phase noise for DU systems obtained in this chapter, i.e., Eqs. (3.39)-(3.40), with the nonlinear phase noise of the DM systems obtained in (Kumar, 2009), i.e., Eqs. (2.28). As it can be seen, for the first few spans there are almost the same, which is due to the insignificant impact of the nonlinear

phase noise compared to the linear phase noise. As we move further through the line, nonlinear phase noise in DM systems starts to dominate the linear phase noise, and for long haul systems it is the main cause of the system degradation, if the deterministic nonlinear phase noise effects are compensated for using DBP. However, in DU systems, linear phase noise is the most dominant noise and it is much smaller than the nonlinear phase noise that is present in the DM systems.

3.5 Conclusions

We have developed an analytical expression for the linear and nonlinear phase noise for the DU fiber optic transmission systems. We have assumed that the ASE noise field added by the inline amplifiers can be accurately described by two DOFs, when we use the matched filter with its bandwidth equal to the signal's bandwidth. Our results have shown that increasing dispersion in the line reduces the phase noise variance at the receiver.

Chapter 4

Fiber Bragg Grating (FBG)

4.1 Introduction

In the previous chapter, we stressed that, in DM systems, in which we compensate for the pulse broadening occuring in each span using a DCF (that is called managing the dispersion), nonlinear phase noise grows exponentially for long haul systems. Then, we showed that, by not managing the dispersion throughout the line and letting the pulse to continue broadening until the end of the line, and compensating for the whole broadening at the end (typically, in electrical domain), gives significant improvement in regards to the nonlinear phase noise variance.

In this chapter we use this concept and go one step further, by adding even more broadening at each span with the help of FBGs (Please see Sec. 1.3.2). We show that adding more dispersion to the propagating signal will reduce the nonlinear phase noise even more, leading to bit error rate (BER) reduction. However, this improvement becomes insignificant for systems with high symbol rates. We will illustrate that systems with different symbol rates need different amounts of accumulated dispersion

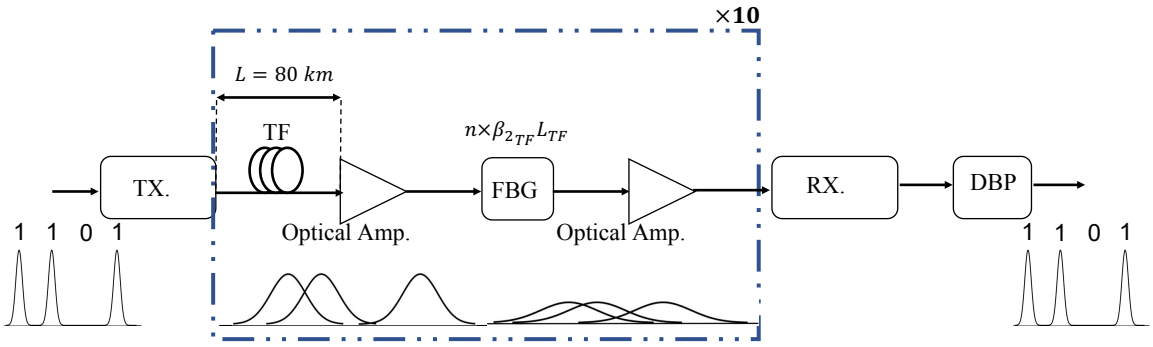

Figure 4.1: Fiber-optic system setup. There is no dispersion compensation within the line. DBP = digital back propagation, TF = transmission fiber. The dispersion added by FBG differs for systems using different symbol rates. $L = 80\ km$.

provided by FBG, or FBG parameter, to perform most effectively.

4.2 System Setup

In this chapter, we use the system configuration as shown in Fig. 4.1. We launch a random sequence of raised cosine pulses as the input signal with average power P. There are 10 spans in our model, each with length of $80km$. Each span includes one $80km$ transmission fiber with positive dispersion value, with loss equal to $16dB$, two EDFAs with each $9dB$ gain, and an FBG with $2dB$ loss. Therefore, the two amplifiers compensate for all the losses due to fiber, and FBG. We assume that the accumulated dispersion provided by FBG is tunable and we find the optimum FBG parameter as a function of symbol rate. We use QAM-256 as our modulation constellation. We use digital back propagation (DBP) at the receiver to compensate for the dispersive and nonlinear effects. It also removes the deterministic nonlinear phase (the second term in Eq. (3.34)) of the received signal. We also use two polarizations to send information.

4.3 Simulation Results

In this section we will illustrate the numerical simulation results of the channel model shown in Fig. 4.1 for symbol rates 5, 10, 15, and 20 GBaud. We will include the simulation results for BER and nonlinear phase noise variance. Figures 4.2 to 4.7 show the BER for different FBG parameters. For example, $n = 1.5$, means that the FBG adds accumulated dispersion equal to 1.5 times the accumulated dispersion added by the $80km$ TF, which is, $\beta_{2_{TF}} L_{TF}$, so the dispersion added by an FBG is $2.5 \times \beta_{2_{TF}} L_{TF}$.

We assume the following parameters throughout this chapter: $\gamma = 0.8\ W^{-1}km^{-1}$, $\alpha_{TF} = 0.2\ dB/km$, EDFA spontaneous noise factor $n_{sp} = 1.5$, and one span length is 80 km. We use transmission fiber with anomalous dispersion between inline amplifiers.

4.3.1 BER and Nonlinear Phase Noise

Fig. 4.2 depicts the BER for different FBG parameters. At lower launch powers, we can see that there is no improvement in the BER, that is because nonlinear phase noise is small compared to other noises. As we increase the launch power, nonlinear phase noise contribution gets larger. In this example, $n = 0$, which means no FBG is the line, has the highest BER. As n increases, we get lower BER, and we have the best systems performance when $n = 2.5$. For the FBG parameters greater than 2.5, the BER starts to go higher, which implies that $n = 2.5$ is the optimum FBG parameter for this case.

Fig. 4.3 illustrates the nonlinear phase noise variance of the transmission system operating at 5 GBaud, when the launched power is 10 dBm. As mentioned earlier,

we are using two polarizations to send information, namely polarization x and polarization y, and since the trend in both of them is similar, therefore, we only present results for polarization x. Fig. 4.3, shows the same trend for the nonlinear phase noise variance, as that for BER, as were expected, because the larger the nonlinear phase noise, the higher the BER. the phase variance is calculated as follows: we compute the phase difference between transmitted signal and the received signal after passing through DBP, for all the 16384 symbols we have sent, and then we calculate its variance. Suppose $\mathbf{Y}$ is the transmitted signal at the input and $\hat{\mathbf{Y}}$ is the signal at the output of the DBP, we find

$$\Phi = \angle\hat{\mathbf{Y}} - \angle\mathbf{Y}, \tag{4.1}$$

$$\text{var}(\Phi) = \sum_{m=1}^{m=16384} \phi_m^2 - \text{mean}(\Phi), \tag{4.2}$$

where

$$\text{mean}(\Phi) = \frac{\sum_{m=1}^{m=16384} \phi_m}{16384}. \tag{4.3}$$

As we increase the symbol rate, the optimum FBG value drops down gradually, and as it can be seen from Fig. 4.4, at around 10 GBaud, $n = 0$, i.e., having no FBG in the line, has the best performance. Fig. 4.5, illustrates the nonlinear phase noise for our system operating at 10 GBaud, and shows that the nonlinear phase noise of the system with no FBG is the minimum, which is consistent with the BER shown in Fig. 4.4.

As we increase the symbol rate further more, we observe that the optimum FBG becomes a negative value, and then goes up and becomes positive again. So, we see a sinc-like behavior in its trend (Please see Sec. 4.4 for more details). It is also

worthy to note that, for higher symbol rates, the improvement gets less significant compared to lower symbol rates. For example, as it can be seen in Fig. 4.6 that the improvement by adding the FBG is less than that in 5 GBaud case. In symbol rates above 20 GBaud, the FBG does not help (Fig. 4.8) to improve the performance.

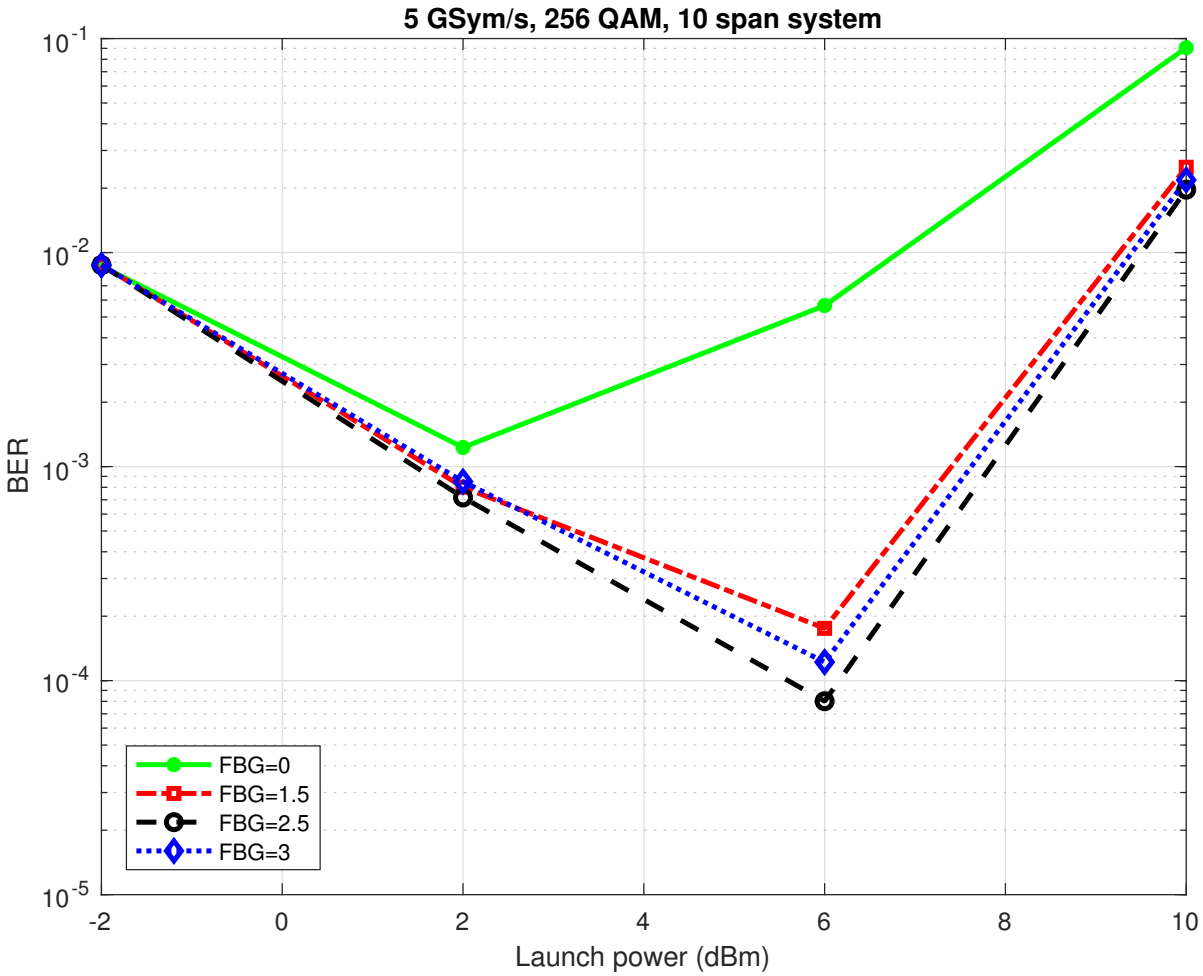

Figure 4.2: Bit error rate (BER) for system model in Fig. 4.1 for various FBG values. Symbol rate: 5 GBaud, and total length is 800 kms.

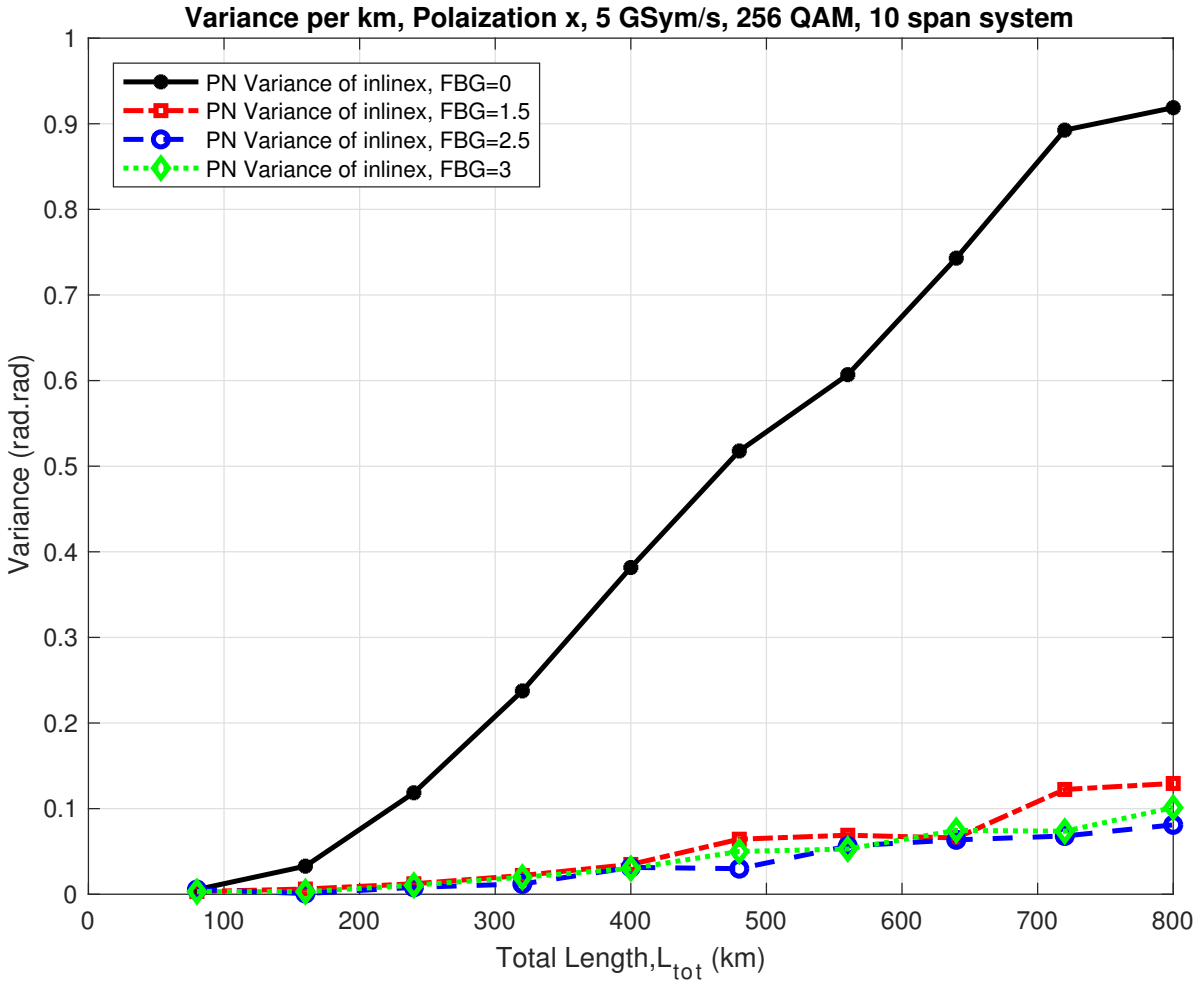

Figure 4.3: Nonlinear phase noise for system model in Fig. 4.1 for various FBG values. Symbol rate: 5 GBaud, P=10 dBm and total length is 800 kms.

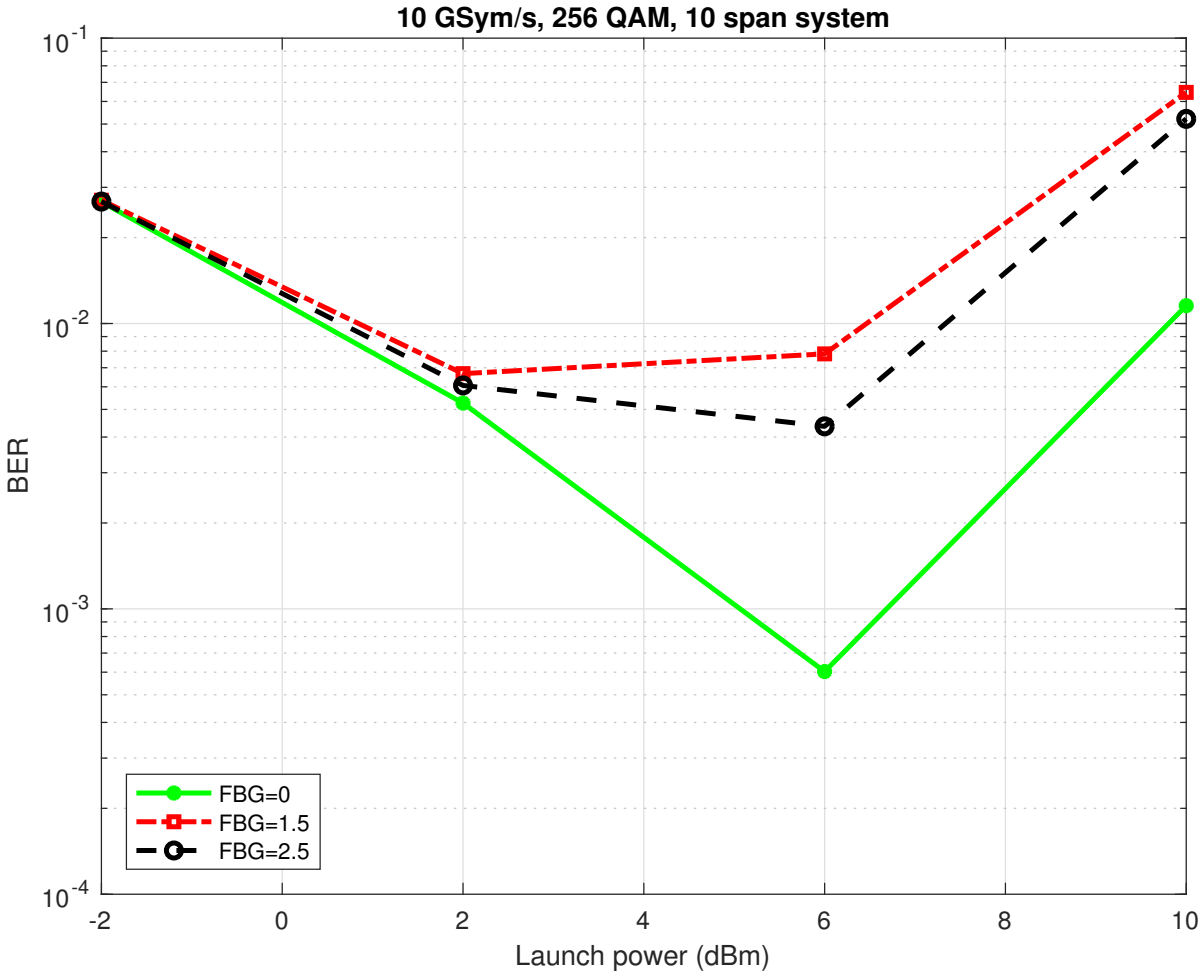

Figure 4.4: Bit error rate (BER) for system model in Fig. 4.1 for various FBG values. Symbol rate: 10 GBaud, and total length is 800 kms.

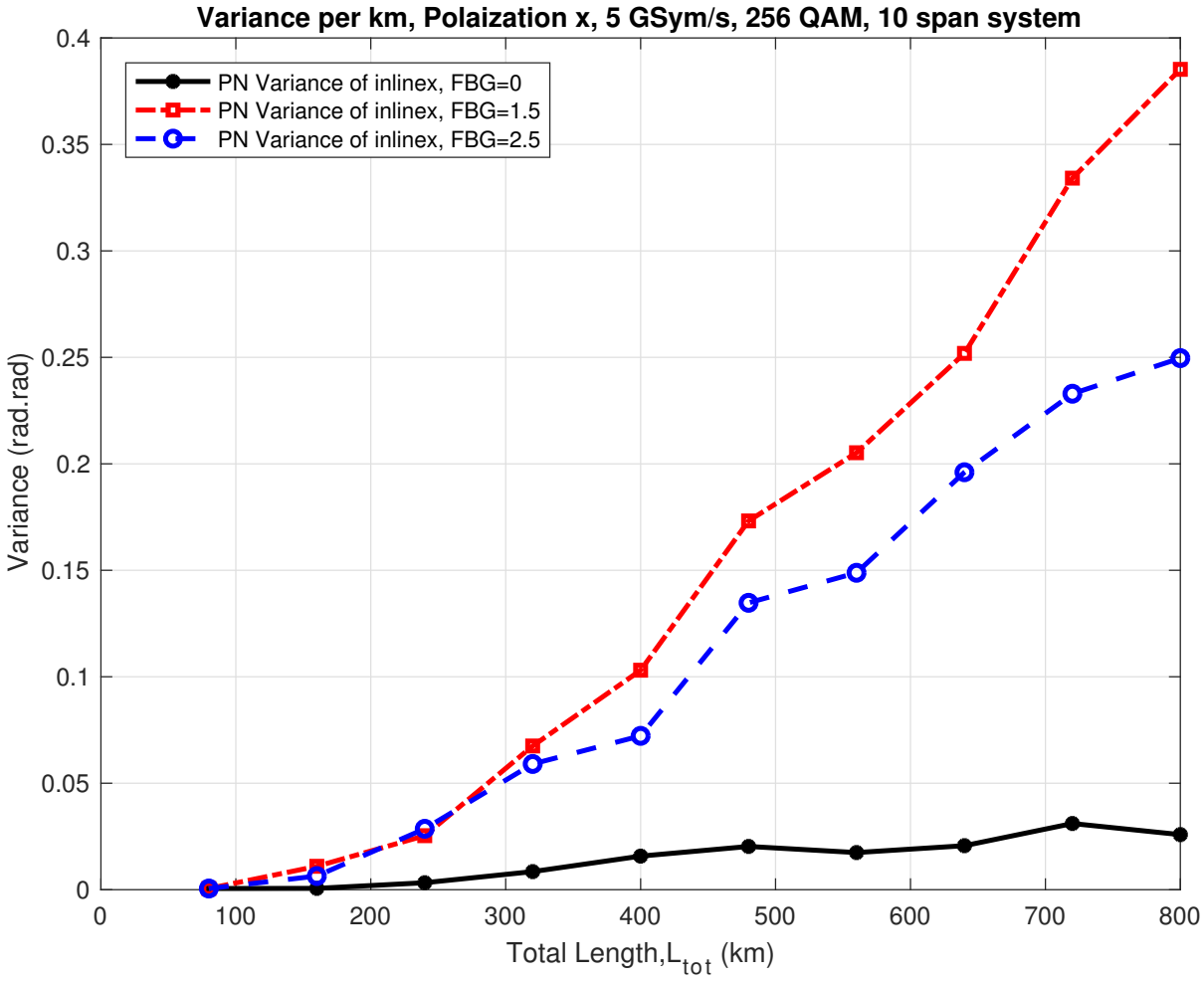

Figure 4.5: Nonlinear phase noise for system model in Fig. 4.1 for various FBG values. Symbol rate: 10 GBaud, P=10 dBm and total length is 800 kms.

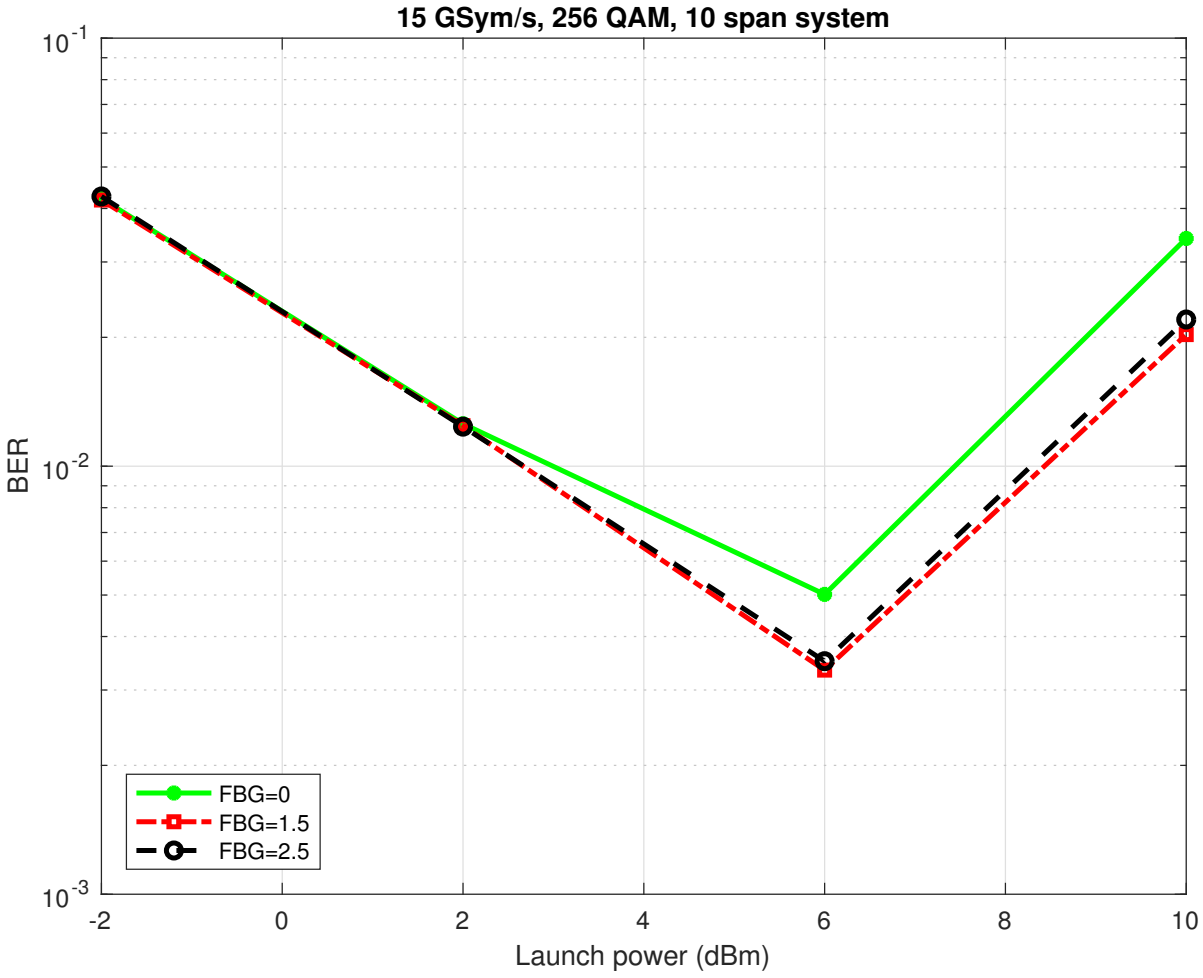

Figure 4.6: Bit error rate (BER) for system model in Fig. 4.1 for various FBG values. Symbol rate: 15 GBaud, and total length is 800 kms.

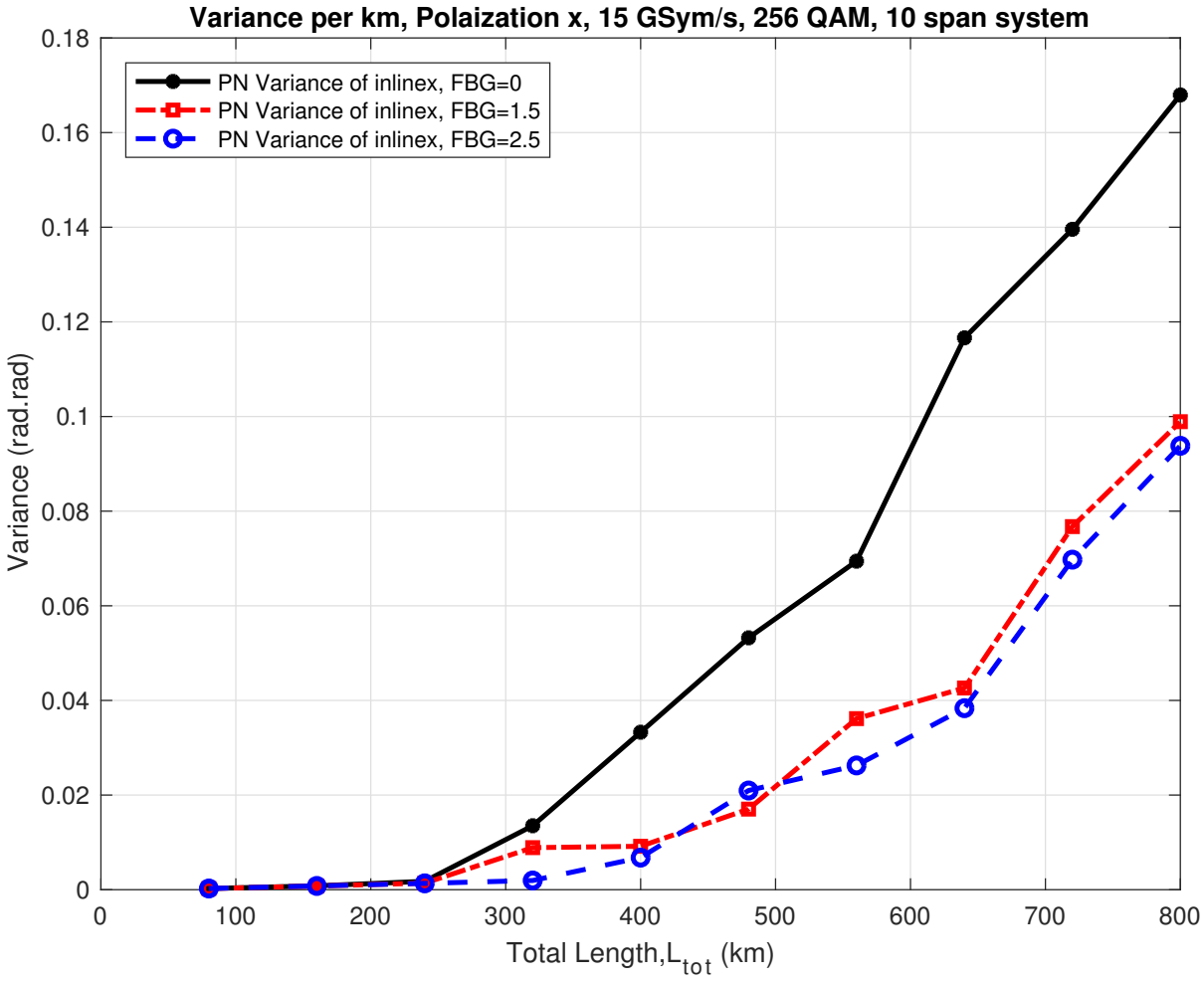

Figure 4.7: Nonlinear phase noise for system model in Fig. 4.1 for various FBG values. Symbol rate: 15 GBaud, P=10 dBm and total length is 800 kms.

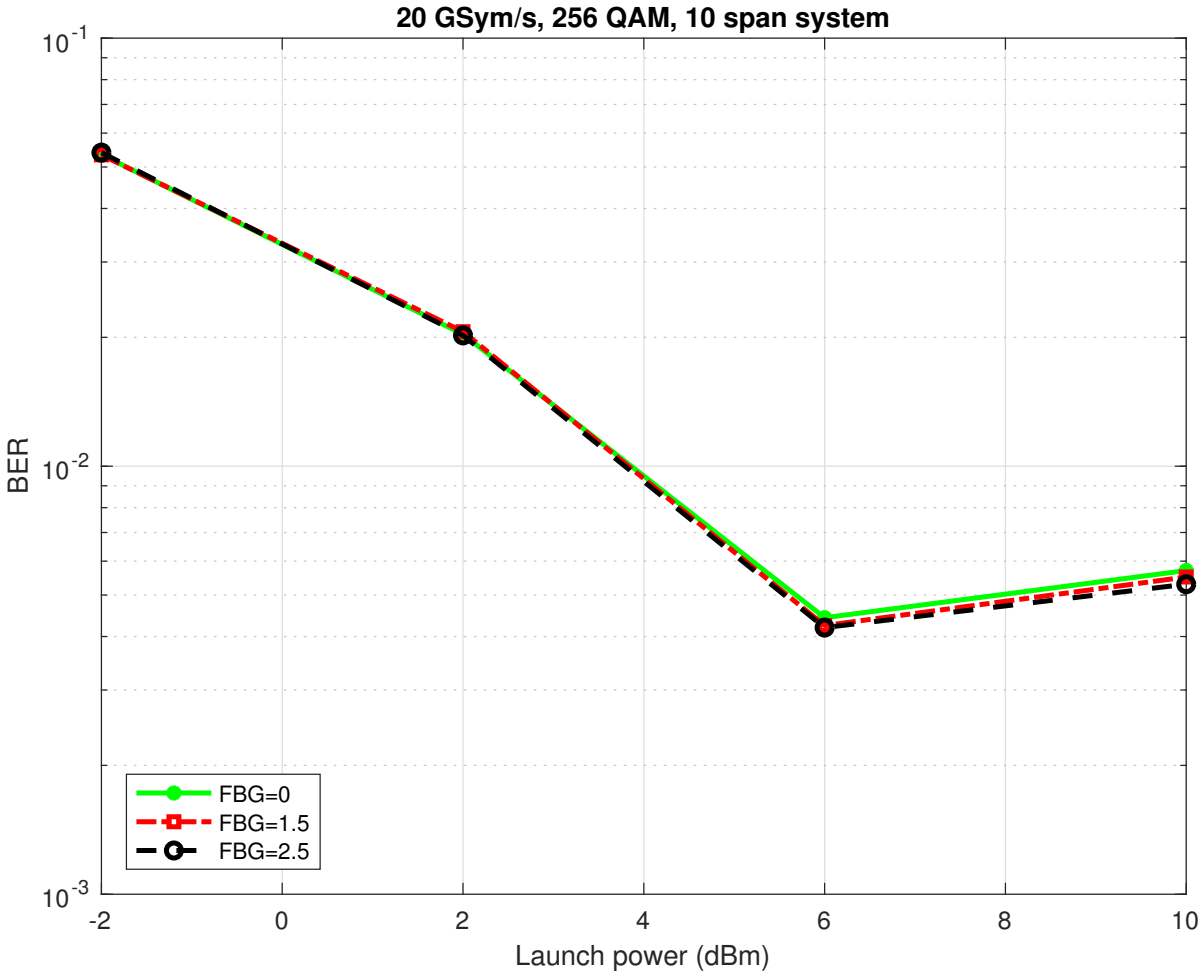

Figure 4.8: Bit error rate (BER) for system model in Fig. 4.1 for various FBG values. Symbol rate: 20 GBaud, and total length is 800 kms.

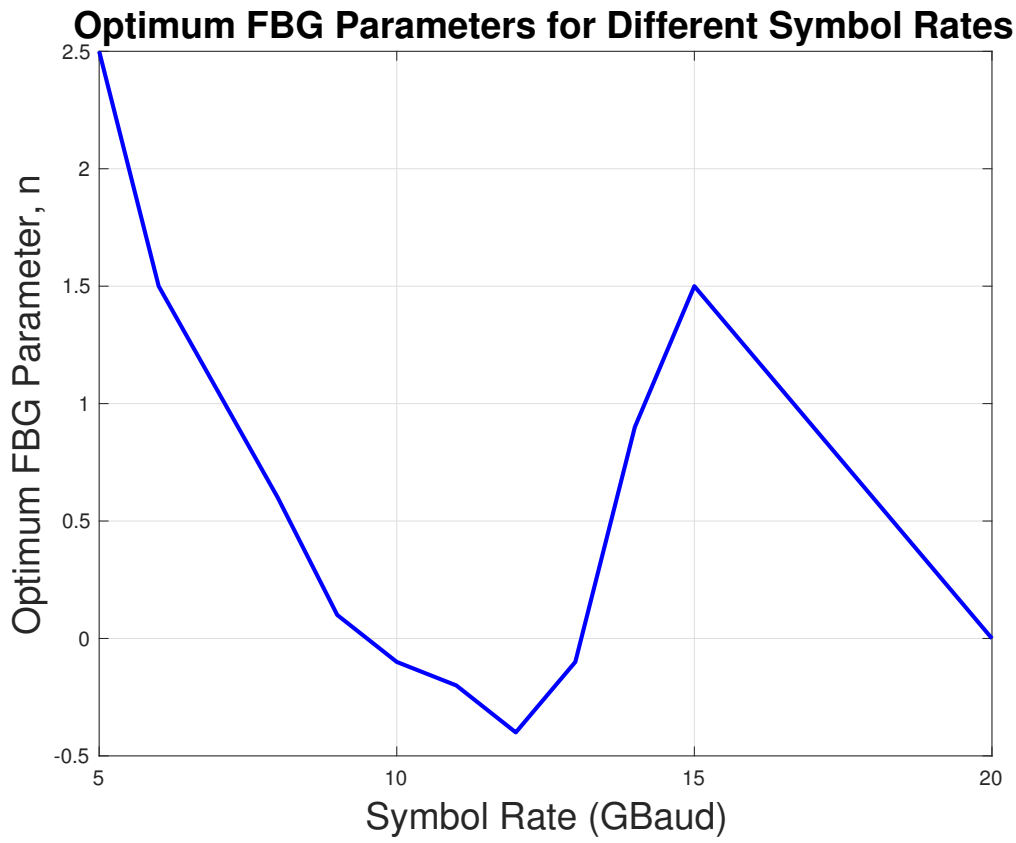

Figure 4.9: Optimum FBG parameters for different symbol rates. Launched power is P=6 dBm, and dispersion parameter of the TF is $|D|$=4 ps/nm.km.

4.4 Optimum FBG

As discussed in Sec. 4.3.1, the optimum FBG value differs by changing the symbol rate. It shows a trend almost like a sinc function. Fig. 4.9 shows that for some symbol rates, negative FBG parameter n has the best performance, which means that in those symbol rates, we should compress signal a little. However, this compression does not compensate for the whole broadening happened through the TF, but for 30% of it at most. For symbol rates higher than 20 GBaud., the improvement by adding FBG is negligible.

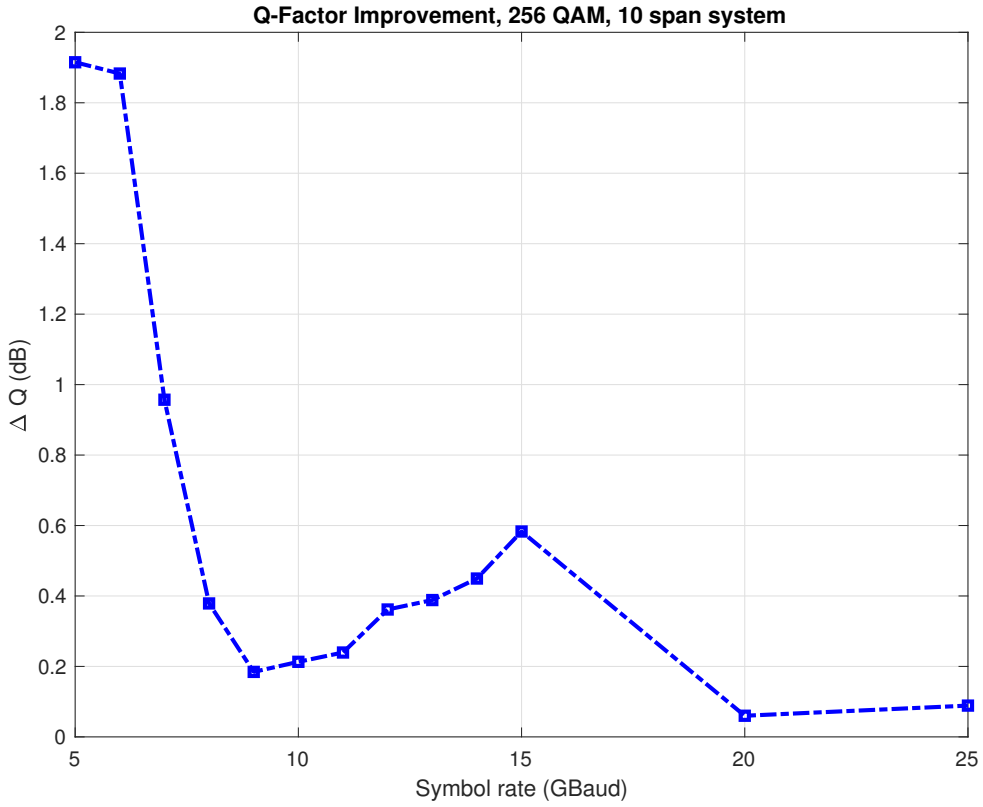

Figure 4.10: System performance improvement in terms of Q-Factor for different symbol rates. $\Delta Q = Q_{opt.} - Q_{stan.}$, where $Q_{opt.}$ is the Q-Factor obtained by system set-up using optimum FBG parameter, i.e., n, and $Q_{stan.}$ is the Q-Factor obtained by standard system set-up without FBG, i.e. $n = 0$. Launched power is P=6 dBm, and dispersion parameter of the TF is $|D|$=4 ps/nm.km.

Figure 4.10 shows the improvement in Q-factor as a function of the symbol rate using the optimum FBG parameter n. As it can be seen in Fig. 4.10, using FBG in the line improves the system performance for some symbol rate range, in terms of Q-factor. Fig. 4.10 shows that we have about 2 dB, and 0.6 dB improvement for systems working at 5 GBaud, and 15 GBaud symbol rates, respectively.

4.5 conclusion

In this chapter, we introduced a new system model, in which we used fiber brag gratings (FBGs) to introduce more dispersion to the line. We have used numerical simulations to illustrate that insertion of FBG with optimum FBG parameter decreases nonlinear phase noise variance and therefore, bit error rate (BER) improves. We showed that systems operating at different symbol rates need different amounts of accumulated dispersion provided by FBG. We found that the improvement in BER gets smaller as the symbol rate increases, and it becomes zero after 20 GBaud. The highest performance improvement of about 2 dB in Q-factor is obtained at a symbol rate of 5 GBaud. The FBG parameter (which is proportional to its accumulated dispersion) is optimized for each symbol rate, and it is found to have a sinc-type dependence on the symbol rate.

Chapter 5

Nonlinear Phase Noise Reduction Using OPC and DBP Distribution

5.1 Introduction

In the previous chapters, we discussed that compensating for the dispersion in each span increases the nonlinear phase noise exponentially, so the DU systems are less prone to this noise, and we derived the nonlinear phase noise variance for DU systems. Then we concluded that pulse broadening throughout the line reduces this variance, therefore, we used FBGs in the line to broaden it even more, and we expected to see more improvements in system performance. Through some numerical simulations, we illustrated that, adding FBG helps to reduce nonlinear phase noise in some symbol rates, but not at all data rates. We got the best improvement at 5 GBaud for FBG parameter of about 2.5, as we increased the symbol rate, we observed that the optimal FBG parameter changes. The simulations showed a sinc-like trend for FBG parameter as a function of symbol rate. We also observed that in higher data rates the

performance improvement becomes less significant, and there was no improvement at symbol rates above 20 GBaud.

Nowadays, practical systems are working at data rates as high as 28 GBaud. In this chapter, we propose a new system model that improves the system performance at this symbol rate. The new set-up splits the DBP used in previous model (see Fig. 4.1), and use them at transmitter and receiver. We will also use optical phase conjugation (OPC) in the line to reduce the nonlinear phase noise further more (Kumar and Liu, 2007). We will discuss different configurations and compare their performance, both analytically and numerically. In the following we will present the configurations that we have considered, and we will derive their nonlinear phase noise variance analytically. Then, we will illustrate the system performance for these configurations by numerical simulations using Q-factor plots.

5.2 Mathematical analysis of the nonlinear phase noise

Consider the fiber optic system shown in Fig. 5.1. Let the signal pulse launched to this system be

$$q(0,t) = Af(t), \tag{5.1}$$

where A^2 is the signal energy, and $f(t)$ is the normalized pulse shape, i.e., $\int |f(t)|^2 = 1$. For simplicity, we ignore fiber dispersion. In the presence of dispersion, the variance obtained here has to be multiplied by a factor that depends on the dispersion map (Kumar and Yang, 2005) and (Kumar, 2009). The signal at the output of the first amplifier is

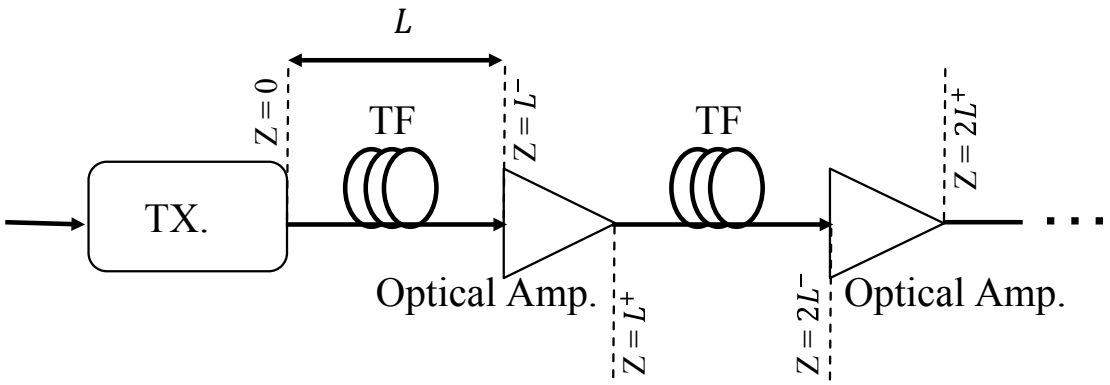

Figure 5.1: Close-up representation of a fiber-optic communication link.

$$q(L^+, t) = Af(t)e^{j\gamma|f(t)|^2 L_{eff} A^2} + n_1(t), \tag{5.2}$$

where α is the fiber loss coefficient, γ is the fiber nonlinear coefficient, $n_1(t)$ is the noise field envelope due to the first amplifier, L is the fiber length, and $L_{eff} = [1 - \exp(-\alpha L)]/\alpha$.

Following the approach of Gordon and Molleneuer (Gordon and Mollenauer, 1990), the noise may be written as

$$n_1(t) = \delta A_1 f(t) e^{j\theta_{n_1}(t)}. \tag{5.3}$$

Substituting (5.3) in (5.2), we obtain

$$q(L^+, t) = (A + \delta A_1) f(t) e^{j\gamma|f(t)|^2 L_{eff} A^2 + j\theta_{n_1}(t)}. \tag{5.4}$$

From (5.4), we see that δA_1 represents the amplitude change due to amplifier noise and $\theta_{n_1}(t)$ represents the linear phase noise. After propagating through the second span, the optical field envelope is

$$q(2L^-,t) = (A+\delta A_1)\, f(t) e^{-\alpha L/2 + j\theta_{n_1}(t)} e^{j\gamma |f(t)|^2 \left[A^2 L_{eff} + (A+\delta A_1)^2 L_{eff}\right]}. \tag{5.5}$$

In Eq. (5.5), the first and second terms in the square bracket, represent the nonlinear phase change due to the first and second fiber spans, respectively. We assume that $\delta A_1 << A$, and approximate $(A+\delta A_1)^2$ as $A^2 + 2A\delta A_1$. Using this, Eq. (5.5) may be rewritten as

$$q(2L^-,t) \cong (A+\delta A_1)\, f(t) e^{-\alpha L/2 + j\theta_{n_1}(t)} e^{j\gamma |f(t)|^2 L_{eff} \left[2A^2 + 2A\delta A_1\right]}. \tag{5.6}$$

5.2.1 Scheme 1: full DBP at the receiver (standard configuration)

Figure 5.2 shows the fiber optic systems consisting of N spans of fibers and inline amplifiers, and a full DBP at the receiver. We refer to this scheme as the standard configuration. Using the procedure outlined in Sec. 5.2, the optical field envelope at the output of the fiber optic link is

$$q(NL^+,t) = \left(A + \sum_{m=1}^{N} \delta A_m\right) f(t) e^{j\theta_n(t) + jK(t)\left(NA^2 + 2A\sum_{m=1}^{N}(N-m)\delta A_m\right)}, \tag{5.7}$$

where,

$$\theta_n(t) = \sum_{i=1}^{N} \theta_{n_i}(t), \tag{5.8}$$

$$K(t) = \gamma |f(t)|^2 L_{eff}. \tag{5.9}$$

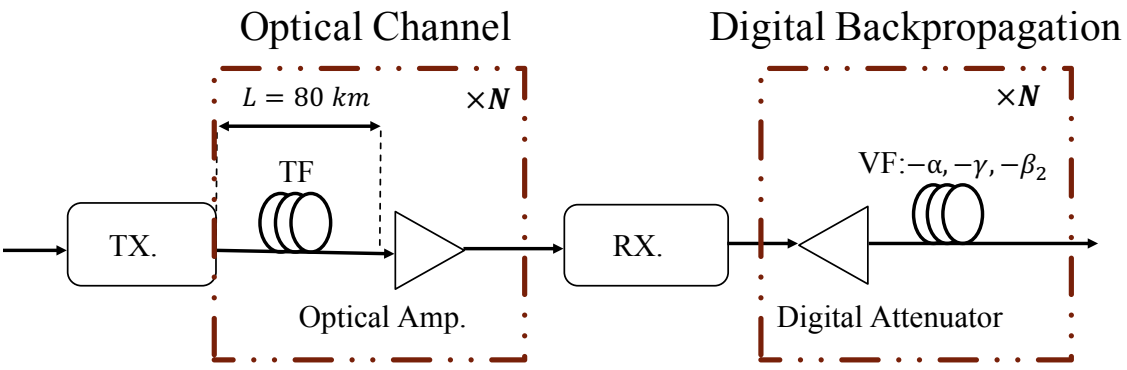

Figure 5.2: Scheme 1: Full DBP at the receiver. The standard configuration. TF stands for transmission fiber, and VF stands for the virtual fiber.

In Eq. (5.7), the first term in the square bracket represents the deterministic nonlinear phase shift due to SPM, whereas the second term represents the stochastic nonlinear phase change due to SPM-ASE interaction. In principle, DBP can mitigate the deterministic nonlinear phase shift. However, the second term is stochastic in nature, and it is hard to compensate for it. The main focus of this chapter is to compare the variance of this stochastic nonlinear phase change in various system configurations.

Let the input of the DBP be the output of the fiber optic link, i.e., $q_b(0,t) = q(NL^+,t)$. Here, the subscript"b" denotes the signal in back propagation. After passing through an attenuator and first span of virtual fiber, the signal is

$$q_b(L^+,t) = \left(A + \sum_{m=1}^{N} \delta A_m\right) f(t) e^{j\theta_n(t) + jK(t)\left((N-1)A^2 + 2A\sum_{m=1}^{N}(N-m-1)\delta A_m\right)}. \quad (5.10)$$

From the first term in the square bracket of Eq. (5.10), it may be noted that the first virtual fiber compensated for the deterministic nonlinear phase change due to the last span of the transmission fiber, and the second term in the square bracket of Eq.

(5.10) shows the modification in the multiplication factor of the stochastic nonlinear phase change. Proceeding in this way, the signal at the output of DBP is

$$q_b(NL^+,t) = \left(A + \sum_{m=1}^{N} \delta A_m\right) f(t) e^{j\theta_n(t) - j2AK(t)\left(\sum_{m=1}^{N} m\delta A_m\right)}. \tag{5.11}$$

Comparing Eq. (5.7) and Eq. (5.11), we note that deterministic nonlinear phase change (KNA^2) is removed by the DBP. At the end of the fiber optic link, nonlinear phase noise $\Big(2AK(t)(N-1)\delta A_1$ in Eq. (5.7)$\Big)$ due to the first inline amplifier has the highest contribution, whereas it has the least contribution after the DBP $\Big(2AK(t)\delta A_1$, in the phase term in Eq. (5.11)$\Big)$.

The nonlinear phase noise after the DBP is,

$$\delta\phi_{NL_1} = -2AK(t)\left(\sum_{m=1}^{N} m\delta A_m\right). \tag{5.12}$$

Assuming that the noises of inline amplifiers are statistically independent, the variance can be added leading to the following expression for the total variance of nonlinear phase noise in the presence of DBP,

$$\sigma^2_{NL_1} = <\delta\phi^2_{NL_1}> = (2AK(t))^2\left(\sum_{m=1}^{N} m^2 < \delta A^2_m >\right). \tag{5.13}$$

For a more rigorous derivation, a factor that depends on the dispersion map has to be included in Eq. (5.13) (Kumar, 2005). However, in this chapter we are mainly interested in the scaling of the phase variation with distance and omit that term. Simplifying Eq. (5.13), we find

$$\sigma^2_{NL_1} \propto (2AK)^2 N^3. \tag{5.14}$$

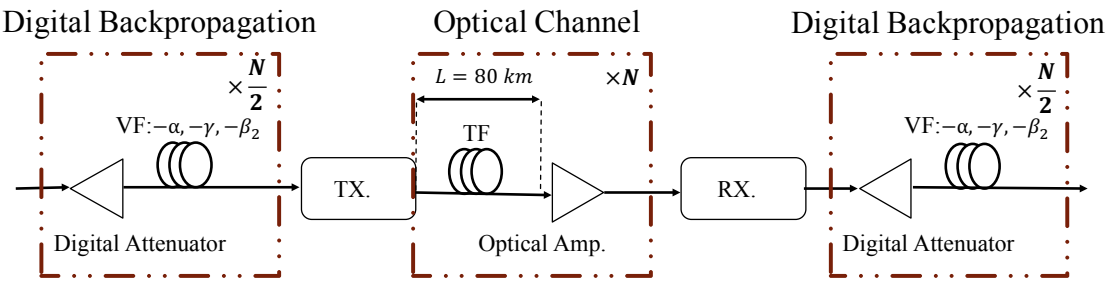

Figure 5.3: Scheme 2: split DBP at the transmitter and the receiver set-up.

For WDM or OFDM systems, stochastic nonlinear phase change due to XPM (Chiang *et al.*, 1996), and FWM (Zhu and Kumar, 2010), becomes important. However, the scaling of the variance with the number of spans would remain the same in the presence of XPM or FWM and hence, we ignore those terms in this study.

5.2.2 Scheme 2: symmetric DBP split between transmitter and receiver (Split DBP)

Figure 5.3 shows the scheme in which the DBP at the transmitter compensates for the propagation impairments of the first half of the fiber optic link, while the DBP at the receiver compensates for the other half. This scheme is referred as split-DBP (Lavery *et al.*, 2016). Proceeding as before, the signal at different system stages is

$$q_b\left(\frac{NL^+}{2},t\right) = Af(t)e^{-jK(t)\frac{N}{2}A^2}, \tag{5.15}$$

$$q\left(NL^+,t\right) = (A+\sum_{m=1}^{N}\delta A_m)f(t)e^{j\theta_n(t)}e^{jK(t)(\frac{N}{2}A^2+2A\sum_{m=1}^{N}(N-m)\delta A_m)}, \tag{5.16}$$

$$q_b\left(NL^+,t\right) = \left(A+\sum_{m=1}^{N}\delta A_m\right)f(t)e^{j\phi_{NL_2}(t)+j\theta_n(t)}, \tag{5.17}$$

where the nonlinear phase noise is

$$\phi_{NL_2}(t) = 2AK(t) \sum_{m=1}^{N} \left(\frac{N}{2} - m \right) \delta A_m. \tag{5.18}$$

Consider the subsystem consisting of the second half of the fiber optic link and the DBP at the receiver. This subsystem is the same as the standard configurations except that the number of spans in this subsystem is $N/2$. Hence, we expect that nonlinear phase noise due to the N^{th} amplifier (δA_N) is the strongest. However, its strength (i.e., multiplication factor) is only $N/2$ (see Eq. (5.18)), since the length of this subsystem is $NL/2$, whereas the strength of the nonlinear phase noise due to N^{th} amplifier is N in the standard configuration. Figure 5.4 compares the absolute value of multiplication factor (or strength) of the nonlinear phase noise due to inline amplifiers for various system configurations.

The variance of nonlinear phase noise can be found using Eq. (5.18) as before,

$$\sigma^2_{NL_2} \propto (2AK(t))^2 \left(\frac{N^3}{4} \right). \tag{5.19}$$

Comparing Eqs. (5.19) and (5.14), we find that the variance of nonlinear phase noise decreases by a factor of 4 for the case of the split-DBP. From Fig. 5.4, we see that for split-DBP, the inline amplifiers located close to the middle of the link do not contribute much to the nonlinear phase noise and the peak multiplication factor drops by a factor of 2 as compared to the case of the standard configuration.

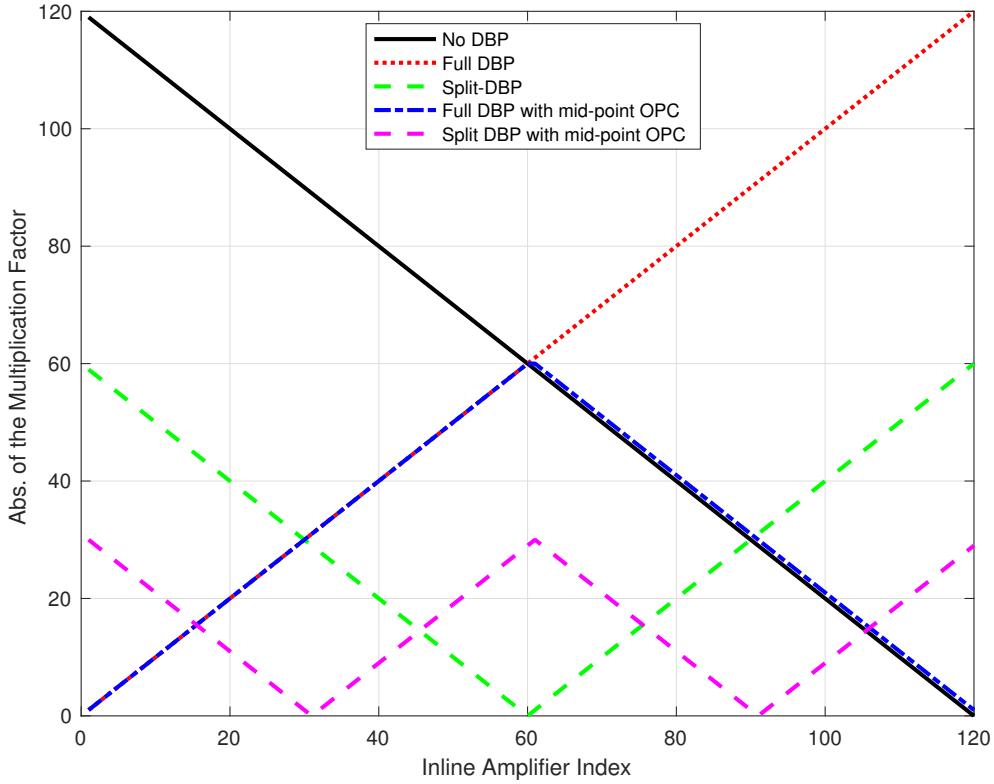

Figure 5.4: Multiplication Factor

5.2.3 Scheme 3: full DBP at the receiver with mid-point OPC

Figure 5.5 shows the system with mid-point OPC and DBP at the receiver. The DBP consists of $N/2$ spans of virtual fibers and attenuators followed by DPC, and $N/2$ spans of virtual fibers and attenuators. The output of the fiber optic link with mid-point OPC is

$$q\left(\frac{NL^{-}}{2},t\right)=\left(A+\sum_{m=1}^{\frac{N}{2}}\delta A_m\right)f(t)e^{jK(t)\left(\frac{N}{2}A^2+2A\sum_{m=1}^{\frac{N}{2}}\left(\frac{N}{2}-m\right)\delta A_m\right)}, \tag{5.20}$$

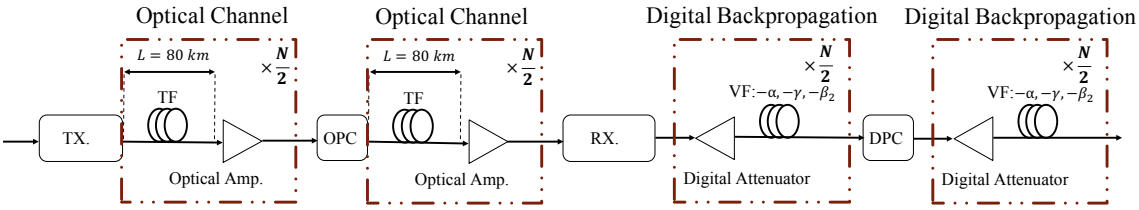

Figure 5.5: Scheme 3: Full DBP at the receiver with OPC set-up.

$$q\left(\frac{NL^+}{2},t\right)=q^*\left(\frac{NL^-}{2},t\right), \tag{5.21}$$

$$q\left(NL^+,t\right)=\left(A+\sum_{m=1}^{N}\delta A_m\right)f(t)e^{j(\phi_1+\phi_2)}, \tag{5.22}$$

where,

$$\phi_1=-K(t)\left(\frac{N}{2}A^2+2A\sum_{m=1}^{\frac{N}{2}}\left(\frac{N}{2}-m\right)\delta A_m\right), \tag{5.23}$$

$$\phi_2=K(t)\left(\frac{N}{2}A^2+2A\frac{N}{2}\sum_{m=1}^{\frac{N}{2}}\delta A_m+2A\sum_{m=\frac{N}{2}+1}^{N}(N-m)\delta A_m\right), \tag{5.24}$$

$$q\left(NL^+,t\right)=\left(A+\sum_{m=1}^{N}\delta A_m\right)f(t)e^{j\theta_n(t)+j2AK(t)\left[\sum_{m=1}^{\frac{N}{2}}m\delta A_m+\sum_{m=\frac{N}{2}+1}^{N}(N-m)\delta A_m\right]}. \tag{5.25}$$

The first and second terms in the square bracket in Eq. (5.25) represent the nonlinear phase noise due to the amplifiers prior to OPC and after OPC, respectively. The nonlinear phase noise due to amplifiers after the OPC are unaffected by OPC and hence,

the second term in the square bracket in Eq. (5.25) is the same as the corresponding terms in Eq. (5.7). Multiplication factor m in the first term can be explained as follows. Consider the m^{th} amplifier ($m \leq N/2$). The OPC may be interpreted as a temporal mirror located at $NL/2$. The nonlinear phase noise source of mL is located at a distance of $(N/2 - m)\, L$ from the mirror, and it has the temporal image at $[N/2 + (N/2 - m)]\, L = (N - m)L$. The temporal image propagates a distance of $[N - (N - m)]L = mL$ leading to a nonlinear phase shift of $K(t)mL(A + \delta A_m)^2$.

After passing through the DBP, the signal is

$$q_b\left(\frac{NL^-}{2}, t\right) = \left(A + \sum_{m=1}^{N} \delta A_m\right) f(t) e^{j(\phi_1+\phi_2)} e^{-jK\left(\frac{N}{2}A^2 + 2A\frac{N}{2}\sum_{m=1}^{N}\delta A_m\right)}, \tag{5.26}$$

$$q_b\left(\frac{NL^+}{2}, t\right) = q_b^*\left(\frac{NL^-}{2}, t\right) \tag{5.27}$$

$$q_b\left(NL^+, t\right) = \left(A + \sum_{m=1}^{N} \delta A_m\right) f(t) e^{j\theta_n(t) + \delta\phi_{NL_3}(t)}, \tag{5.28}$$

where,

$$\delta\phi_{NL_3} = -2AK(t)\left[\sum_{m=1}^{\frac{N}{2}} m\delta A_m + \sum_{m=\frac{N}{2}+1}^{N} (N - m)\, \delta A_m\right]. \tag{5.29}$$

It may be noted that the peak of the multiplication factor is $N/2$ similar to the case of split-DBP. Using Eq. (5.29), nonlinear phase noise variance is calculated as

$$\sigma_{NL_3}^2 \propto (2AK)^2 \left(\frac{N^3}{4}\right). \tag{5.30}$$

Comparing Eqs. (5.14) and (5.30), we find that the variance decreases by a factor of

4 using the mid-point OPC as compared to the standard configuration. Hence, the nonlinear phase noise reduction factor is the same for mid-point OPC scheme with the receiver DBP (scheme 3) and split DBP (scheme 2).

5.2.4 Scheme 4: split DBP at transmitter with mid-point OPC

In this section, we split DBP between transmitter and receiver and combine this technique with mid-point OPC to further reduce the nonlinear phase noise. Figure 5.6 shows the system configuration. The DBP at the transmitter and receiver compensate for the propagation impairment due to the first $N/4$, and the remaining $3N/4$ of the amplifiers, respectively. The DBP at the receiver consists of $N/2$ spans of virtual fibers and attenuators followed by DPC, and $N/4$ spans of virtual fibers and attenuators. The output of the fiber optic link with split DBP and mid-point OPC is

$$q_b\left(\frac{NL^+}{4},t\right)=Af(t)e^{-jK(t)\frac{N}{4}A^2}, \tag{5.31}$$

$$q\left(\frac{NL^-}{2},t\right)=\left(A+\sum_{m=1}^{\frac{N}{2}}\delta A_m\right)f(t)e^{jK(t)\left(\frac{N}{4}A^2+2A\sum_{m=1}^{\frac{N}{2}}\left(\frac{N}{2}-m\right)\delta A_m\right)}, \tag{5.32}$$

$$q\left(\frac{NL^+}{2},t\right)=q^*\left(\frac{NL^-}{2},t\right) \tag{5.33}$$

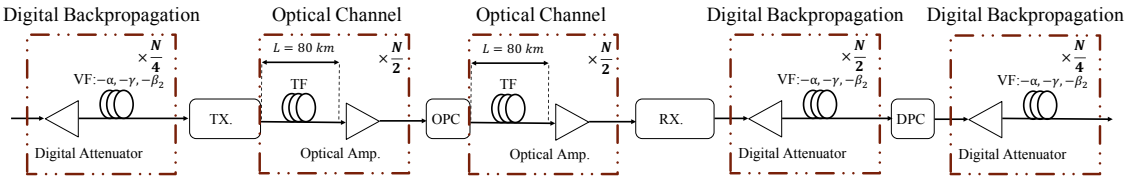

Figure 5.6: Scheme 4: Fiber optic system with a mid-point OPC and asymmetric DBP

$$q(NL^+,t)=\left(A+\sum_{m=1}^{N}\delta A_m\right)f(t)e^{j\theta_n(t)+jK(t)A^2\frac{N}{4}+j2AK(t)\left[\sum_{m=1}^{\frac{N}{2}}m\delta A_m+\sum_{m=\frac{N}{2}+1}^{N}(N-m)\delta A_m\right]}. \tag{5.34}$$

The second term in the exponential term in Eq. (5.34) represents the deterministic phase change added by the transmitter-side DBP. The system configuration between transmitter and the receiver, which includes N TFs and amplifiers, and a mid-point OPC, resembles the corresponding subsystem in scheme 2. Therefore, the same reasoning for the terms inside the bracket in Eq. (5.25) can be applied to the terms inside the bracket in Eq. (5.34).

$$q_b\left(\frac{NL^-}{2},t\right)= \left(A+\sum_{m=1}^{N}\delta A_m\right)f(t)e^{-jK(t)\left(\frac{N}{4}A^2+2A\sum_{m=1}^{\frac{N}{2}}\left(\frac{N}{2}-m\right)\delta A_m-2A\sum_{m=\frac{N}{2}+1}^{N}\left(\frac{N}{2}-m\right)\delta A_m\right)}, \tag{5.35}$$

$$q_b\left(\frac{NL^+}{2},t\right)=q_b^*\left(\frac{NL^-}{2},t\right). \tag{5.36}$$

The output of the DBP is

$$q_b\left(NL^+,t\right)=\left(A+\sum_{m=1}^{N}\delta A_m\right)f(t)e^{j\theta_n(t)+\delta\phi_{NL_4}(t)}, \tag{5.37}$$

where,

$$\delta\phi_{NL_4} = -2KA\left[\sum_{m=1}^{\frac{N}{2}}\left(m-\frac{N}{4}\right)\delta A_m + \sum_{m=\frac{N}{2}+1}^{N}\left(\frac{3N}{4}-m\right)\delta A_m\right]. \tag{5.38}$$

The first and second terms in inside the square bracket represent the stochastic nonlinear phase shift due to the amplifiers before and after the mid-point OPC, respectively. It may be noted that, as Fig. 5.4 shows, the multiplication factors have two peaks at $N/2$ and N, due to using mid-point OPC, as discussed in scheme 3, and DBP, as discussed in scheme 2, respectively. Depending on how we distribute the DBP between the transmitter and the receiver, the peak value can differ. For example, splitting the DBP by half, results in the peak value of $N/2$. Figure 5.6 shows the optimum distribution of the DBP, in which the peak value is $N/4$.

Using Eq. (5.38), we find the nonlinear phase noise,

$$\sigma^2_{NL_4} \propto (2AK)^2\left(\frac{N^3}{16}\right). \tag{5.39}$$

Comparing Eq. (5.39) with Eqs. (5.14), (5.19), and (5.30), we find that the variance decreases by a factor of 16 and 4 using split-DBP and mid-point OPC, compared to standard configuration and schemes 2 and 3.

5.3 Numerical Simulations

In this section we provide numerical examples to compare the performance of the system configurations discussed in Sec. 5.2. The simulations include both dual polarization (DP) single channel and DP-WDM with 5 channel transmission systems,

and we study the performance in terms of Q-factor. The Q-factor is calculated using (Kumar and Deen, 2014),

$$Q = 20log_{10}\left(\sqrt{2}erfcinv\left[2.BER\right]\right), \tag{5.40}$$

where the BER is the bit error rate computed by the error counting. We use the following parameters: dispersion coefficient β_2 =$-21ps^2/km$, loss coefficient α =$0.2dB/km$, nonlinear coefficient γ =$1.1W^{-1}km^{-1}$, symbol rate=28 GBaud, amplifier noise figure, NF= 4.77dB, channel spacing=50 GHz, and amplifier spacing is 80km. QAM-16 has been used as the modulation format for all simulations. Raised cosine pulses with the rolling factor= 0.2 are used. Number of symbols simulated= 16384 in each polarization. Simulation bandwidths are 123.2 GHz and 308 GHz, respectively, for single channel and WDM systems. The fiber optic system as well as DBP are modeled by Manakov equations (Wai and Menyak, 1996). The split-step Fourier scheme (Agrawal, 2012), (Kumar and Deen, 2014), is used to solve the Manakov equations. The step size is so chosen that the peak nonlinear phase accumulated in each step is 0.04 rad. The number of samples per symbol are 8 and 20, respectively, for single channel and WDM systems.

5.3.1 Single Channel Systems

Figure 5.7 compares the system performance of the four schemes. For all the four schemes, the Q-factor drops at higher launch powers. This is because, although deterministic (and symbol-pattern dependent) nonlinear impairments are compensated for by the DBP, stochastic nonlinear impairments can not be fully compensated for. For the standard configuration, the optimum launch power is 6 dBm, which shifts to

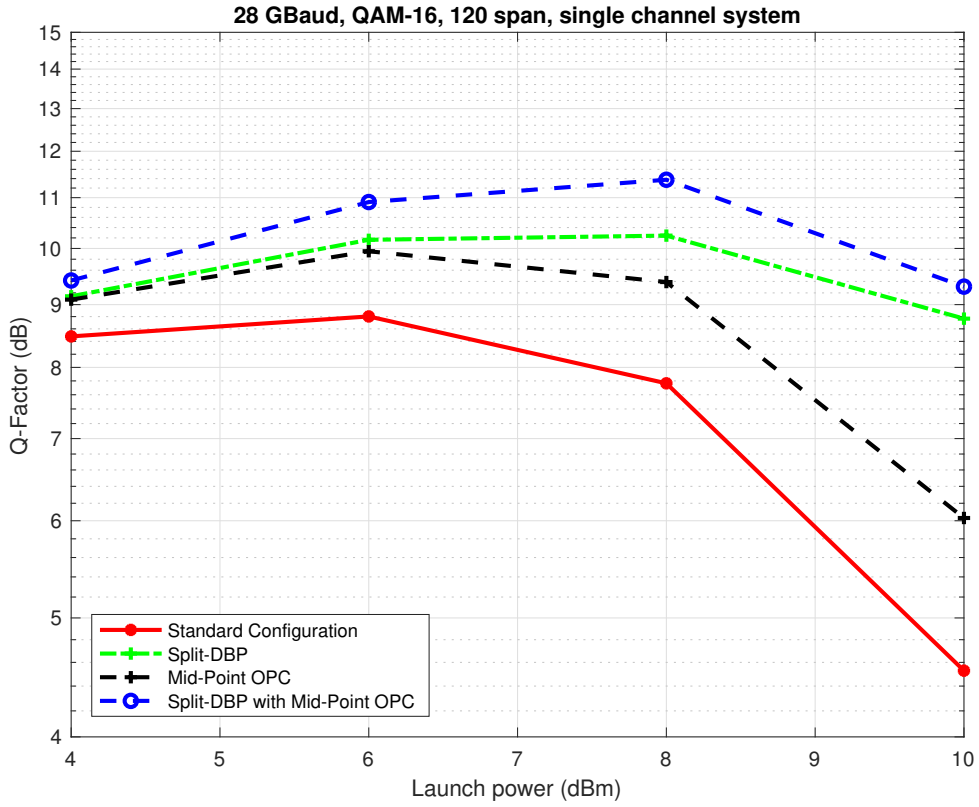

Figure 5.7: Q-factor performance comparison of the four schemes, for single channel systems.

8 dBm for the case of split-DBP. Also, the optimum Q-factor improves by 1.44 dB for split-step as compared to the standard configuration, consistent with the theoretical model of Secs. 5.2.1 and 5.2.2. Reference (Lavery *et al.*, 2016) also showed the improvemnt in Q-factor using split-DBP. However, the improvement was not attributed to reduction in stochastic nonlinear phase shift. Figure 5.7 shows that by combining split-DBP with mid-point OPC, the Q-factor improves by 2.6 dB as compared to standard configuration. However, simple model of Sec. 5.2.4 predicts an improvement of $\sim$6 dB for scheme 4 at higher launch powers when the nonlinear phase noise

is the dominant impairment, but the simulations shows only 4.78 dB improvement at a launch power of 10 dBm. This discrepancy can be explained as follows. The simple model in Secs. 5.2.3 and 5.2.4 ignores fiber dispersions. Under this condition, the fiber span located at $(N/2+m)L$, compensates exactly for the nonlinear distortion due to the fiber span located at $(N/2-m)L$. However, in the presence of dispersion, this compensation is not exact due to fiber loss, i.e., power symmetry with respect to OPC location is broken. Hence, the temporal image at $(N-m)L$ of a nonlinear phase noise source at mL (see Sec. 5.2.3) is not exact, which leads to higher nonlinear phase noise variance than that predicted by Eq. 5.39. If the distributed Raman amplifiers are used instead of EDFAs, power-symmetry with respect to OPC location can be maintained and we should expect a higher optimum Q-factor for schemes 3 and 4 in this scenario. This would be the subject of future investigation.

5.3.2 Five-Channel WDM Systems

To mitigate nonlinear impairments of a WDM system, we use the full DBP approach (Li *et al.*, 2008). The central channel is de-multiplexed after the DBP using an ideal bandpass filter of full bandwidth 31.5 GHz. Figure 5.8 shows the Q-factor as a function of launch power for various system configurations. WDM results have the same trend as that of single-channel systems. Split-DBP (scheme 2) and split-DBP with mid-point OPC (scheme 4) proved Q-factor improvements of 1.55 dB and 2.14 dB, respectively, as compared to the standard configuration.

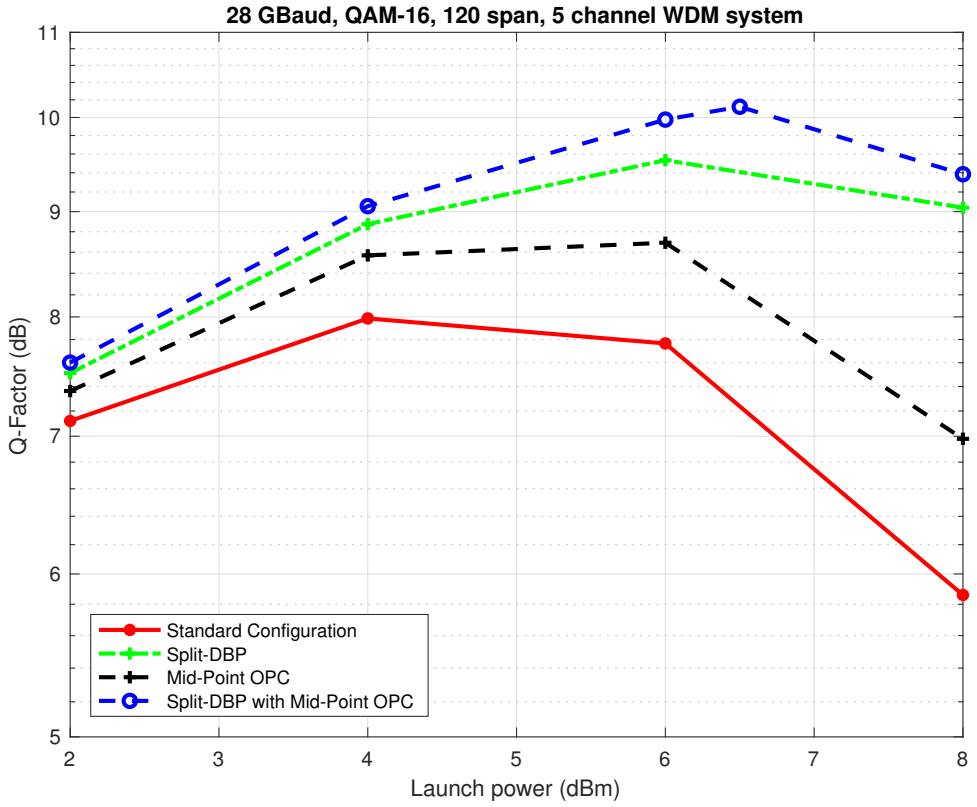

Figure 5.8: Q-factor performance comparison of the four schemes, for WDM system with 5 channels.

5.4 conclusion

The introduction of optical fibers into communication systems at the beginning and then the advent of coherent receivers and optical amplifiers have opened the doors of huge data transmission over a very long (continental) distances. However, many imperfections hinder us to achieve the full capacity of the fiber optic systems, and many studies have addressed various problems and proposed their ideas to tackle them. In this chapter, we have proposed a new scheme to reduce the nonlinear phase noise variance, which caused in the performance improvement. We derived analytical

expressions for the nonlinear phase noise variance, for standard system configuration, which consists of a multi-span fiber optic lines with lumped amplifiers, and digital back propagation (DBP) at the receiver, that compensates for the dispersion and deterministic nonlinearity, caused by signal-signal beating due to the well-known Kerr effect. The proposed system configuration, splits the DBP between the transmitter and the receiver, with %25 being at the transmitter side, and also uses mid-line OPC to defeat the nonlinear impairments. Analytical derivations show that, this technique reduces the nonlinear phase noise variance by a factor of 16 compared to standard configuration and by a factor of 4 compared to half-DBP split, and mid-line OPC without DBP splitting. Numerical simulations illustrated this concept, in both single channel systems and 5-channel-WDM systems. We have seen about 2.6dB and 2dB improvement in Q-factor, compared to standard configuration, in single channel systems and WDM systems, respectively, for 9600km fiber line.

Chapter 6

Conclusion and Future Work

The introduction of optical fibers into communication systems at the beginning and then the advent of coherent receivers and optical amplifiers have opened the doors of huge data transmission over a very long (continental) distances. There have been many obstacles that scientists and researches have overcame to increase the transmission capacity further, and as for now data rate of about five tera bits per second is achieved, which is three to five orders of magnitude greater than that the previous means of transmission could achieve. Despite these advancements, there are still numerous challenges we need to cope with. This study deals with a stochastic noise called nonlinear phase noise, which is due to the interaction of the noise added by the inline optical amplifiers and the nonlinearity within the fiber.

Chapters 1 and 2 gave a brief introduction and literature review about the subject. In chapter 1, we began with the history of optical fibers and its advancement and emphasized on the necessity of this research. We talked about their numerous applications which telecommunication was among them. Then we elaborated more on fiber optic communication systems, their impairments, and the optical components.

Then we gave a brief history and literature review about important concepts that we needed for this study. In chapter 2, we talked about the mathematical foundation of this study. We introduced the famous nonlinear *Schrödinger* equation (NLSE), which governs the pulse propagation inside the fiber, and we talked about the methods to solve it. Afterwards, we introduced the dispersion managed (DM) systems and practiced the procedure to derive the nonlinear phase noise variance for Gaussian inputs, which was the base for our work, except we did not compensate for the dispersion.

In chapter 3, we studied dispersion unmanaged systems and derived an analytical expression for the linear and nonlinear phase noise and its variance. We discussed that using 2 DOFs to describe the ASE noise field added by the inline amplifiers is sufficient, we use the matched filter with its bandwidth equal to the signal's bandwidth. Then, we used numerical simulations to illustrate that increasing dispersion in the line reduces the phase noise variance at the receiver.

In chapter 4, we proposed a new model to introduce more dispersion to the propagating signal in line, using fiber brag gratings (FBGs). We presented numerical examples to show the performance of this model, in terms of nonlinear phase noise variance and BER. We saw that the noise variance decreased for some extra accumulated dispersion value added by FBG , which we called FBG parameter, and therefore, BER got improved. However, we deduced that this improvement is the highest for 5 GBaud, and for higher symbol rates we saw less betterment. We illustrated that there is no improvement for symbol rates above 20 GBaud. We showed there is a since type dependence for optimum FBG parameter in terms of symbol rate.

In chapter 5, we studied various fiber optic communication system configurations

and proved analytically that the nonlinear phase nose variance reduces for these set-ups compared to the standard configuration. In these schemes we split the DBP between receiver and transmitter, and we also used mid-point OPC within the line. Then, through numerical examples we confirmed this improvement for QAM-16, for symbol rate equal to 28 GBaud, in terms of Q-factor. We observed about 2.6 dB and 2 dB improvement in Q-factor for single channel and WDM with 5 channel systems for total length of 9600 kms.

Appendix A

Nonlinear Field Derivation

Continuing from Eq. (3.21), we have

$$j\frac{\partial \tilde{u}_1(z,\omega)}{\partial z} + \alpha(z)\tilde{u}_1(z,\omega) = -p(z,\omega), \quad z > L_m, \tag{A.1}$$

where

$$\alpha(z,\omega) = \frac{\beta_2(z)\omega^2}{2}, \tag{A.2}$$

$$p(z,\omega) = \gamma \exp(-w(z))\mathcal{F}\left(|u_0(z,\omega)|^2 u_0(z,\omega)\right), \tag{A.3}$$

Using Eqs. (3.16)-(3.20), we have

$$\mathcal{F}\left(|u_0(z,\omega)|^2 u_0(z,\omega)\right) = \mathcal{F}\left(c(z)\exp\left(-R(z)t^2\right)\right), \tag{A.4}$$

$$= c(z)\int_{-\infty}^{+\infty}\exp\left(-R(z)t^2 - j\omega t\right)dt, \tag{A.5}$$

$$= c(z)\sqrt{\frac{\pi}{R(z)}}\exp\left(-\frac{\omega^2}{4R(z)}\right), \tag{A.6}$$

$$p(z,\omega) = \gamma(z)\exp(-w(z))c(z)\sqrt{\frac{\pi}{R(z)}}\exp\left(-\frac{\omega^2}{4R(z)}\right). \tag{A.7}$$

For the integration in Eq. (A.5) we have used

$$\int_{-\infty}^{+\infty}\exp\left(-at^2 - bt\right)dt = \sqrt{\frac{\pi}{a}}\exp\left(\frac{b^2}{4a}\right), \tag{A.8}$$

We find

$$j\frac{\partial\tilde{u}_1}{\partial z} + \alpha(z,\omega)\tilde{u}_1 = -p(z,\omega), \quad z > L_m, \tag{A.9}$$

$$d\tilde{u}_1 - j\alpha(z,\omega)\tilde{u}_1 dz = jp(z,\omega)dz, \quad z > L_m, \tag{A.10}$$

$$d\tilde{u}_1 + \tilde{u}_1 d\left(-j\int_{L_m}^{z}\alpha(s,\omega)ds\right) = jp(z,\omega)dz, \quad z > L_m, \tag{A.11}$$

$$e^{j\int_{L_m}^{z}\alpha(s,\omega)ds} d\left(\tilde{u}_1 e^{-j\int_{L_m}^{z}\alpha(s,\omega)ds}\right) = jp(z,\omega)dz, \quad z > L_m, \tag{A.12}$$

$$d\left(\tilde{u}_1 e^{-j\int_{L_m}^{z}\alpha(s,\omega)ds}\right) = je^{-j\int_{L_m}^{z}\alpha(s,\omega)ds}p(z,\omega)dz, \quad z > L_m, \tag{A.13}$$

$$\tilde{u}_1 e^{-j\int_{L_m}^{z}\alpha(s,\omega)ds} = j\int_{L_m}^{z} e^{-j\int_{L_m}^{y}\alpha(s,\omega)ds}p(y,\omega)dy, \quad z > L_m, \tag{A.14}$$

So we have:

$$\tilde{u}_1(z,\omega) = je^{j\overbrace{\int_{L_m}^{z}\alpha(s,\omega)ds}^{\frac{1}{2}\omega^2 S(z)}}\int_{L_m}^{z} e^{-j\overbrace{\int_{L_m}^{z}\alpha(s,\omega)ds}^{\frac{1}{2}\omega^2 S(y)}}p(y,\omega)dy, \tag{A.15}$$

$$\tilde{u}_1(z,\omega) = j\int_{L_m}^{z}\exp\left(j\frac{1}{2}\omega^2(S(z)-S(y))\right)p(y,\omega)dy. \tag{A.16}$$

Substituting Eq. (A.7) in Eq. (A.16), and setting $z = L_T$, we find

$$\begin{aligned}\tilde{u}_1(z=L_T,\omega) =& j\int_{L_m}^{L_T}\underbrace{\gamma(y)\exp(-w(y))c(y)\sqrt{\frac{\pi}{R(y)}}}_{D(y)}\exp\left(j\frac{1}{2}\omega^2(S(L_T)-S(y))\right)\\ &\times\exp\left(-\frac{\omega^2}{4R(y)}\right)dy,\end{aligned} \tag{A.17}$$

$$= j\int_{L_m}^{L_T}\underbrace{\gamma(y)\exp(-w(y))c(y)\sqrt{\frac{\pi}{R(y)}}}_{D(y)}\exp\left(-\underbrace{\left(\frac{1}{4R(y)}-j\frac{1}{2}(S(L_T)-S(y))\right)}_{\Delta_1(y)}\omega^2\right)dy, \tag{A.18}$$

$$\tilde{u}_1(L_T,\omega) = j\int_{L_m}^{L_T} D(y)\exp\left(-\Delta_1(y)\omega^2\right)dy. \tag{A.19}$$

Now, taking inverse Fourier transform will give us the nonlinear portion of the propagating field

$$u_1(L_T,t) = \frac{1}{2\pi}j\int_{L_m}^{L_T} D(y)\int_{-\infty}^{+\infty}\exp\left((-\Delta_1(y)\omega^2 + jt\omega\right)d\omega dy, \tag{A.20}$$

$$u_1(L_T,t) = \frac{j}{2\pi}\int_{L_m}^{L_T} D(y)\sqrt{\frac{\pi}{\Delta_1(y)}}\exp\left(-\frac{t^2}{4\Delta_1(y)}\right)dy \tag{A.21}$$

In the intergration in Eq. (A.20) we gave used the relation in Eq. (A.8). By setting $D(y)$ and $\Delta_1(y)$ we have:

$$u_1(L_T,t) = j\int_{L_m}^{L_T} \underbrace{\frac{\gamma(y)\exp(-w(y))c(y)}{\sqrt{1-j2R(y)(S(L_T)-S(y))}}}_{A(L_T,y)}\exp\left(-\underbrace{\frac{R(y)}{1-j2R(y)(S(l_T)-S(y))}}_{\Delta(y)}t^2\right)dy \tag{A.22}$$

Therefore, we find

$$u_1(L_T,t) = j\int_{L_m}^{L_T} A(L_T,y)\exp\left(\Delta(y)t^2\right)dy, \tag{A.23}$$

where

$$A(L_T,y) = \frac{\gamma\exp(-w(y))c(y)}{\sqrt{1-j2R(y)(S(L_T)-S(y))}}, \tag{A.24}$$

$$\Delta(y) = \frac{R(y)}{1 - j2R(y)(S(L_T) - S(y))}. \tag{A.25}$$

Appendix B

Matched Filter Output Derivation

Continuing from Eq. (3.31), and using Eq. (3.30), we have

$$u_f = \int_{-\infty}^{+\infty} u(L_T, t) F^\star(0, t) dt, \tag{B.26}$$

$$u_f = \int_{-\infty}^{+\infty} (n_0 + \sqrt{E}) F(0,t) \times \left[1 + j\sqrt{\frac{E}{P}} \int_{L_m}^{L_T} \frac{A(L_T, y)}{\sqrt{E} + n_0} \exp\left(- \left(\Delta(y) - \frac{1}{2T_0^2} \right) t^2 \right) dy \right] F^\star(0,t) dt, \tag{B.27}$$

$$u_f = \int_{-\infty}^{+\infty} (n_0 + \sqrt{E}) |F(0,t)|^2 \times \left[1 + j\sqrt{\frac{E}{P}} \int_{l_m}^{L_T} \frac{A(L_T, y)}{\sqrt{E} + n_0} \exp\left(- \left(\Delta(y) - \frac{1}{2T_0^2} \right) t^2 \right) dy \right] dt, \tag{B.28}$$

$$u_f = \int_{-\infty}^{+\infty} \frac{P(n_0+\sqrt{E})}{E} \exp\left(-\frac{t^2}{T_0^2}\right) \times \left[1 + j\sqrt{\frac{E}{P}} \int_{L_m}^{L_T} \frac{A(L_T,y)}{\sqrt{E}+n_0} \exp\left(-\left(\Delta(y) - \frac{1}{2T_0^2}\right) t^2\right) dy\right] dt, \tag{B.29}$$

$$u_f = \underbrace{\int_{-\infty}^{+\infty} \frac{P(n_0+\sqrt{E})}{E} \exp\left(-\frac{t^2}{T_0^2}\right) dt}_{I_1} + \overbrace{j\sqrt{\frac{P}{E}} \int_{-\infty}^{+\infty} \int_{L_m}^{L_T} A(L_T,y) \exp\left[-\left(\Delta(y) - \frac{1}{2T_0^2} + \frac{1}{T_0^2}\right) t^2\right] dydt}^{I_2} = I_1 + I_2, \tag{B.30}$$

In the following we will calculate I_1 and I_2.

$$I_1 = \frac{(n_0+\sqrt{E})P}{E} \int_{-\infty}^{+\infty} \exp\left(-\frac{t^2}{T_0^2}\right) dt = \frac{(n_0+\sqrt{E})P}{E} \sqrt{\pi T_0^2} = \frac{(n_0+\sqrt{E})}{\sqrt{\pi} T_0} \sqrt{\pi T_0^2}. \tag{B.31}$$

So we have

$$I_1 = \sqrt{E} + n_0, \tag{B.32}$$

and I_2 can be calculated as

$$I_2 = j\sqrt{\frac{P}{E}} \int_{-\infty}^{+\infty} \int_{l_m}^{l_T} A(l_T,y) \exp\left(-\left(\Delta(y) + \frac{1}{2T_0^2}\right) t^2\right) dydt, \tag{B.33}$$

$$I_2 = j\sqrt{\frac{P}{E}} \int_{l_m}^{l_T} A(l_T,y) \int_{-\infty}^{+\infty} \exp\left(-\left(\Delta(y) + \frac{1}{2T_0^2}\right) t^2\right) dtdy, \tag{B.34}$$

$$I_2 = j\sqrt{\frac{P}{E}}\int_{l_m}^{l_T} A(l_T,y)\sqrt{\frac{\pi}{\Delta(y)+\frac{1}{2T_0^2}}}dy = j\sqrt{\frac{P}{E}}\int_{l_m}^{l_T} A(l_T,y)\sqrt{\frac{2T_0^2\pi}{1+2T_0^2\Delta(y)}}dy. \tag{B.35}$$

So we have

$$I_2 = j\sqrt{\frac{P}{E}}\int_{l_m}^{l_T} A(l_T,y)\frac{\sqrt{2\pi}T_0}{\sqrt{1+2T_0^2\Delta(y)}}dy, \tag{B.36}$$

$$u_f = I_1 + I_2, \tag{B.37}$$

$$u_f = n_0 + \sqrt{E} + j\sqrt{\frac{P}{E}}\int_{l_m}^{l_T} A(l_T,y)\frac{\sqrt{2\pi}T_0}{\sqrt{1+2T_0^2\Delta(y)}}dy, \tag{B.38}$$

$$u_f = n_0 + \sqrt{E} + j\sqrt{\frac{P}{E}}\int_{l_m}^{l_T} \frac{P\sqrt{P}\gamma(y)\exp(-w(y))(\sqrt{E}+n_0)(E+\delta E)T_0^3}{E\sqrt{E}T_2(y)|T_2(y)|^2\sqrt{1-j2R(y)(S(l_T)-S(y))}}\frac{\sqrt{2\pi}T_0}{\sqrt{1+2T_0^2\Delta(y)}}dy, \tag{B.39}$$

$$u_f = (n_0+\sqrt{E})\times \left[1 + \frac{jP^2T_0^2\times\sqrt{\pi}T_0}{E^2}\int_{l_m}^{l_T}\frac{T_0\gamma(y)\exp(-w(y))(E+\delta E)\sqrt{2}}{T_2(y)|T_2(y)|^2\sqrt{(1-j2R(y)(S(l_T)-S(y)))\,(1+2T_0^2\Delta(y))}}dy\right], \tag{B.40}$$

$$u_f = (n_0 + \sqrt{E})\times \left[1 + j\frac{T_0}{\sqrt{\pi}}\int_{l_m}^{l_T} \frac{T_0\gamma(y)\exp(-w(y))(E+\delta E)\sqrt{2}}{T_2(y)|T_2(y)|^2\sqrt{(1-j2R(y)(S(l_T)-S(y)))\,(1+2T_0^2\Delta(y))}}dy\right], \tag{B.41}$$

$$u_f = (n_0 + \sqrt{E})\left[1 + j(E+\delta E)g_{fm}(l_T)\right], \tag{B.42}$$

where,

$$g_{fm}(l_T) = \frac{T_0}{\sqrt{\pi}}\int_{l_m}^{l_T} \frac{T_0\gamma(y)\exp(-w(y))\sqrt{2}}{T_2(y)|T_2(y)|^2\sqrt{(1-j2R(y)(S(l_T)-S(y)))\,(1+2T_0^2\Delta(y))}}dy. \tag{B.43}$$

Bibliography

Agrawal, G. P. (2011). *Fiber-Optic Communication Systems*. John Wiley & Sons, 4 edition.

Agrawal, G. P. (2012). *Nonlinear Fiber Optics*. Academic Press, 5 edition.

AlAmri, M., ElGomati, M., and Zubairy, S. (2016). *Optics in Our Time*, chapter 13, pages 299–333. Springer, Cham.

Almeida, T., Drummond, M., Pavlovic, N., Andr?e, P., and Nogueira, R. (2015). A fast method for launch parameter optimization in long-haul dispersion-managed optical links. *J. Lightw. Technol.*, **33**(20), 4303–4310.

Bass, M. (2001). *Fiber Optics Handbook: Fiber, Devices, and Systems for Optical Communications*. McGraw Hill Professional.

Benzoni, J. and Orletsky, D. (1989). *Military Applications of Fiber Optics Technology*. Rand.

Chiang, T. ., Kagi, N., Marhic, M. E., and Kazovsky, L. G. (1996). Cross-phase modulation in fiber links with multiple optical amplifiers and dispersion compensators. *Journal of Lightwave Technology*, **14**(3), 249–260.

Dakin, J. (1988). *Optical Fiber Sensors: Principles And Components*. Artech House Publishers.

Demir, A. (2007). Nonlinear phase noise in optical fiber communication systems. *J. Lightw. Technol.*, **25**(8), 2002–2032.

Ekanayake, N. and Herath, H. (2013). Effect of nonlinear phase noise on the performance of m-ary psk signals in optical fiber links. *J. Lightw. Technol.*, **31**(3), 447–454.

Favre, F. and D.LeGuen (1980). High frequency stability of laser diode for heterodyne communication systems. *Electron. Lett.*, **16**(18), 709–710.

Gordon, J. P. and Mollenauer, L. F. (1990). Phase noise in photonic communications systems using linear amplifiers. *Opt. Lett.*, **15**(23), 1351–1353.

Griffiths, D. J. (2017). *Introduction to Electrodynamics*. Cambridge University Press, 4 edition.

Guenther, B. D. (2004). *Encyclopedia of Modern Optics*, volume 1. Elsevier Science Publishing Co Inc, 1 edition.

Hill, K. O., Fujii, Y., Johnson, D. C., and Kawasaki, B. S. (1978). Photosensitivity in optical fiber waveguides: Application to reflection filter fabrication. *Appl. Phys. Lett.*, **32**(10), 647–649.

Ho, K. (2003). Probability density of nonlinear phase noise. *J. Opt. Soc. Amer. B*, **20**(9), 1875–1879.

Kawasaki, B. S., Hill, K. O., Johnson, D. C., and Fujii, Y. (1978). Narrow-band bragg reflectors in optical fibers. *Opt. Lett.*, **3**(2), 66–68.

Kikuchi, K. (2011). Digital coherent optical communication systems: fundamentals and future prospects. *IEICE Electro. Express*, **8**(20), 1642–1662.

Kikuchi, K. (2016). Fundamentals of coherent optical fiber communications. *J. Lightw. Technol.*, **34**(1), 157–179.

Kumar, S. (2005). Effect of dispersion on nonlinear phase noise in optical transmission systems. *Opt. Lett.*, **30**(24), 3278–3280.

Kumar, S. (2009). Analysis of nonlinear phase noise in coherent fiber-optic systems based on phase shift keying. *J. Lightw. Technol.*, **27**(21), 4722–4733.

Kumar, S. and Deen, M. J. (2014). *Fiber Optic Communications: Fundamentals and Applications*. John Wiley & Sons.

Kumar, S. and Liu, L. (2007). Reduction of nonlinear phase noise using optical phase conjugation in quasi-linear optical transmission systems. *Opt. Express*, **15**(5), 2166–2177.

Kumar, S. and Yang, D. (2005). Second-order theory for self-phase modulation and cross-phase modulation in optical fibers. *J. Lightw. Technol.*, **23**(6), 2073–2080.

Lavery, D., Ives, D., Liga, G., Alvarado, A., Savory, S. J., and Bayvel, P. (2016). The benefit of split nonlinearity compensation for single-channel optical fiber communications. *IEEE Photonics Technology Letters*, **28**(17), 1803–1806.

Li, X., Chen, X., Goldfarb, G., Mateo, E., Kim, I., Yaman, F., and Li, G. (2008). Electronic post-compensation of wdm transmission impairments using coherent detection and digital signal processing. *Opt. Express*, **16**(2), 880–888.

McGhan, D., Laperle, C., Savehenko, A., Li, C., Mak, G., and O'Sullivan, M. (2005). 5120 km rz-dpsk transmission over g652 fiber at 10 gb/s with no optical dispersion compensation. In *Optical Fiber Communication Conference, (OFC 2005)*, volume 6, page 3 pp., Anaheim, CA, USA, March 6-11. Paper PDP27.

Mears, R. J., Reekie, L., Jauncey, I. M., and Payne, D. N. (1987). Low-noise erbium-doped fibre amplifier at 1.54?m. *Electron. Lett.*, **23**(19), 1026–1028.

Mecozzi, A. (1994). Limits to the long haul coherent transmission set by the kerr nonlinearity and noise of in-line amplifiers. *J. Lightw. Technol.*, **12**(11), 1993–2000.

Mecozzi, A. (2004). Probability density functions of the nonlinear phase noise. *Opt. Lett.*, **29**(7), 673–675.

Mollenauer, L. and Gordon, J. (2006). *Solitons in Optical Fibers: Fundamentals and Applications*. Elsevier/Academic Press.

Okhotnikov, O. G. (2012). *Fiber Lasers*. John Wiley & Sons.

Okoshi, T. and Kikuchi, K. (1980). Frequency stabilization of semiconductor lasers for heterodyne-type optical communication systems. *Electron. Lett.*, **16**(5), 179–181.

Pan, C., Blow, H., Idler, W., Schmalen, L., and Kschischang, F. (2015). Optical nonlinear phase noise compensation for 9×32 -gbaud poldm-16 qam transmission using a code-aided expectation-maximization algorithm. *J. Lightw. Technol.*, **33**(17), 3679–3686.

Sarkis, C. (2009). *Reach Enhancement in both Direct-Detection and Coherent Detection Optical Fiber Communication Systems*. Master's thesis, McMaster University, http://hdl.handle.net/11375/22394.

Singh, S. P. and Singh, N. (2007). Nonlinear effects in optical fibers: Origin, management and applications. *Progress In Electromagnetics Research*, **73**, 249–275.

Tsukamoto, S., Ly-Gagnon, D. S., Katoh, K., and Kikuchi, K. (2005). Coherent demodulation of 40-gbit/s polarization-multiplexed qpsk signals with 16-ghz spacing after 200-km transmission. In *Optical Fiber Communication Conference, (OFC 2005)*, volume 6, page 3 pp., Anaheim, CA, USA, March 6-11. Paper PDP29.

Wai, P. K. A. and Menyak, C. R. (1996). Polarization mode dispersion, decorrelation, and diffusion in optical fibers with randomly varying birefringence. *Journal of Lightwave Technology*, **14**(2), 148–157.

Wang, D., Zhang, M., Li, Z., Cui, Y., Liu, J., Yang, Y., and Wang, H. (2015). Nonlinear decision boundary created by a machine learning-based classifier to mitigate nonlinear phase noise. In *Proc. ECOC*, pages 1–3.

Weng, Z., Chi, Y., Wang, H., Tsai, C., and Lin, G. (2018). 75-km long reach dispersion managed ofdm-pon at 60 gbit/s with quasi-color-free ld. *J. Lightw. Technol.*, **36**(12), 2394–2408.

Xu, Z., Kam, P. Y., and Yu, C. (2014). Adaptive maximum likelihood sequence detection for qpsk coherent optical communication system. *Photon. Technol. Lett.*, **26**(6), 583–586.

Zhu, X. and Kumar, S. (2010). Nonlinear phase noise in coherent optical ofdm transmission systems. *Opt. Express*, **18**(7), 7347–7360.